frontiers | Frontiers in Mechanical Engineering

TYPE Original Research
PUBLISHED 04 November 2025
DOI 10.3389/fmech.2025.1689473

OPEN ACCESS

EDITED BY
Anatoliy Levin,
Melentiev Energy Systems Institute (RAS), Russia

REVIEWED BY
Andrey Chernov,
Institute of Thermophysics (RAS), Russia
Polina Khan,
Melentiev Energy Systems Institute (RAS), Russia

*CORRESPONDENCE
Hamed H. Saber,
saberh@rcjy.edu.sa

RECEIVED 20 August 2025
ACCEPTED 18 September 2025
PUBLISHED 04 November 2025

CITATION
Saber HH (2025) Impact of multidimensional airflow and internal radiation heat exchange in thermally massive wall assemblies utilizing cold-formed steel framing and reflective insulation.
Front. Mech. Eng. 11:1689473.
doi: 10.3389/fmech.2025.1689473

Impact of multidimensional airflow and internal radiation heat exchange in thermally massive wall assemblies utilizing cold-formed steel framing and reflective insulation

Hamed H. Saber *

Jubail Industrial College, Royal Commission of Jubail and Yanbu, Jubail Industrial City, Saudi Arabia

Thermal bridging due to high-conductivity metal elements in steel-framed systems can affect building performance. The presence of thermal bridges, radiative heat exchange between air-facing surfaces, and natural convection driven by buoyancy effects within cavities contribute to complex 3D airflow and heat transfer phenomena within these systems. With the wide range of reflective and mass insulation properties used in steel-framed wall assemblies, this study employs a previously developed and validated 3D numerical model to evaluate the thermal performance of a reflective insulation system (RIS) and a hybrid system that integrates reflective insulation with conventional mass insulation. Additionally, a methodology aligned with ASTM C1224 is introduced for separating the thermal bridging effects of steel framing elements to allow for evaluating the thermal resistances of wall cavities in RIS and hybrid systems. This work demonstrates, for the first time to the author's knowledge, the coupled effects of conduction, convection, radiation, and airflow in steel-framed assemblies incorporating reflective insulation with and without conventional mass insulation. It further identifies a previously unreported critical conductivity threshold where partial and full cavity insulation yield equivalent resistance and provides data to extend current standards that omit RIS. The findings indicate that for mass insulation materials with low thermal conductivity, wall systems in which cavities are completely filled with insulation exhibit greater thermal resistance than those with only partially filled cavities. However, as the thermal conductivity of the insulation increases, the trend reverses, with partially filled cavities providing higher thermal resistance than completely filled ones. There exists a critical thermal conductivity threshold at which the thermal resistance of both configurations becomes equivalent. Beyond this point, wall systems with less insulation in their cavities can achieve superior thermal resistance to those where the cavities are completely filled. Given that existing design guidelines, such as Thermal Design and Code Compliance for Cold-Formed Steel Walls, do not currently address RIS, the data generated in this study provide a foundation for future updates. By integrating RIS and hybrid systems

into thermal design practices, this research supports the development of cost-effective, high-performance steel-framed wall systems that enhance energy efficiency while maintaining material and regulatory compliance.

KEYWORDS

reflective insulation, steel-framed system, emittance, effective *R*-values, thermal bridges

Highlights

- Reflective insulation provides more improvement in thermal resistance with high-conductivity mass insulation.
- Partially filled cavities outperform fully insulated ones when mass insulation has high thermal conductivity.
- A critical conductivity threshold exists where both full and partial insulation provide equal thermal resistance.
- Integrating reflective and mass insulation optimizes energy efficiency and reduces material costs.
- Findings support updates to design guidelines for steel-framed walls incorporating reflective insulation.

Introduction

Different types of thermal insulation are used in the design of building envelope components. Thermal bridging occurs in a building component when a conductive material (e.g., metal) creates a path for heat flow that bypasses different types of thermal insulation. This reduces the thermal performance of the component. Additionally, different configurations of thermal insulation combined with heat-conducting elements create thermal bridging effects in multiple areas of a building's exterior and architectural interfaces. These effects can greatly influence the thermal and moisture performance of building envelopes as well as their durability. Examples of pathways for heat flow caused by specific design features in a building's structure include the following (Kosny and Yarbrough, 2022):

- Reinforced concrete and steel-framed beams and columns.
- Roof rafters and floor joists.
- Framing components made of wood or metal that intersect the thermal insulation.
- Cantilevered structures that penetrate the building envelope.
- Headers and lintels that disrupt the continuity of thermal insulation.
- Connectors linking metal-foam-metal sandwich panels.

Metal framing is made from highly thermally conductive material (e.g., steel or aluminum) compared to traditional wood framing; this study focuses on assessing the performance of steel-framed wall systems. Metal framing is widely used in commercial and residential buildings. However, one of the critical concerns with metal framing is its thermal performance, particularly the issue of thermal bridging. For example, Kosny et al. (1997) conducted a detailed analysis of metal-framed wall assemblies and found that thermal bridging can lead to an increase in cooling and heating loads by up to 30%. Kosny et al. (2007) showed that thermal bridging can account for up to 40% of the total heat transfer in certain scenarios. Because of thermal bridging in some conventional wall systems, the whole-wall thermal resistance (*R*-value) can be as much as 40% less than that of a clear wall (Kośny et al., 2016). In cold Canadian climates, simulations revealed that incorporating thermal bridges raises the yearly heating load by 38%–42% and reduces the yearly cooling load by 8%–26% (Ge and Baba, 2017). Considering that in certain assembly configurations, interface details can affect up to 50% of the entire wall area, the overall *R*-value of the wall can be reduced by up to 40% compared to that of a clear-wall section (Kosny and Desjarlais, 1994)

There is a need for careful design and material selection to minimize the effect of thermal bridging. Various strategies have been employed to mitigate the thermal bridging effect. These include the use of continuous exterior insulation, thermal break materials, and advanced framing techniques. Trethowen (1988) showed that using continuous exterior insulation or incorporating insulated sheathing could significantly mitigate the effect of thermal bridging. Kosny and Yarbrough (2022) demonstrated that the use of continuous exterior insulation can significantly reduce thermal bridging in metal-framed walls, and thus improve their overall thermal performance. A case study by the NAHB Research Center (Barbour et al., 1994) examined a residential building retrofit project that incorporated continuous exterior insulation and thermal breaks, resulting in a 25% improvement in energy efficiency. The use of continuous insulation and thermal breaks to retrofit commercial office buildings led to a 35% reduction in heating and cooling loads (Roppel et al., 2011).

Thermal bridges offer a direct route for heat transfer, which can considerably diminish the insulation efficiency (thermal resistance) of the building's façade. This results in heat escaping from the interior to the exterior during cold weather or entering the interior during hot weather. Such reductions in thermal resistance can cause discomfort within the building and typically increase the energy demand for cooling and heating systems. Furthermore, thermal bridges can cause condensation when warm, moist air encounters cooler surfaces (NCC, 2021). This condensation can lead to mold growth, which deteriorates indoor air quality, poses health risks for occupants, and potentially compromises the structure's durability.

If not properly addressed, the detrimental impact of thermal bridges due to the steel frame can significantly affect the energy performance of light steel frame (LSF) buildings. Over the past few decades, various construction techniques have been explored to enhance the thermal performance of steel-framed systems. These techniques include minimizing the contact area between steel studs and sheathing, slotting steel studs to reduce their area, substituting steel with materials that have lower thermal conductivity, or incorporating elements like foam insulation caps at critical thermal bridge locations. The most widely adopted method to counteract this issue involves applying insulation on the exterior of the steel framework (Gorgolewski, 2007). Subpar interface details can result in significant condensation, leading to unsightly stains and dust accumulation on interior surfaces, which visibly indicate

thermal bridging. Damp areas can also promote the growth of mold, which can reduce indoor air quality (Hens, 2007).

In summary, thermal bridging can lead to several unwanted consequences:

1. Increased energy consumption: Thermal bridges cause heat loss (in the case of heating buildings) or unwanted heat gain (in the case of cooling buildings), significantly raising the overall energy usage.
2. Mold growth: In colder weather, the temperatures in the walls may fall below the dew point, causing condensation. This can result in mold growth, which poses health risks if persistent [see Hens (2007) or Trechsel and Bomberg (2009)].
3. Reduced thermal comfort: Low surface temperatures can make indoor living spaces uncomfortable.

Although some thermal bridging is inevitable due to structural requirements, effective design and construction practices can minimize its presence and mitigate its impact.

Previous research has extensively investigated the impact of thermal bridging on the thermal performance of steel-framed wall systems with mass insulation. However, there is a notable gap in the literature regarding its effect on steel-framed wall systems incorporating reflective insulation (RI), either alone or in combination with mass insulation. To address this gap, the present study systematically evaluates the energy performance of steel-framed wall assemblies integrating various types of RI. Additionally, the research explores configurations that combine RI with different types of mass insulation to provide a comprehensive understanding of their thermal behavior under varying conditions.

While previous research has extensively investigated thermal bridging in steel-framed systems with conventional mass insulation, there remains a significant gap in understanding the combined effects of multidimensional airflow, radiative heat exchange, and thermal bridging in wall systems incorporating reflective insulation systems (RISs) and hybrid insulation systems. To address this gap, the present study introduces a methodology aligned with ASTM C1224 (ASTM, 2021) to separate the thermal bridging effects of steel framing elements from cavity contributions in assemblies containing both an RIS and hybrid systems. A validated 3D model is used to capture the coupled effects of conduction, convection driven by buoyancy-induced airflow, and radiation under standard labeling conditions for an RIS.

This study demonstrates the existence of a critical thermal conductivity threshold at which partially insulated and fully insulated cavities provide the same thermal resistance. To the author's best knowledge, this represents a novel insight not previously reported for steel-framed assemblies incorporating both reflective and conventional mass insulation. Together, these contributions advance the fundamental understanding of reflective and hybrid insulation performance in steel-framed construction and provide essential data that are directly relevant to the development of future design standards and building codes.

RI featuring low-emittance (low-e) surfaces is widely incorporated into building envelope components either independently or in conjunction with conventional mass insulation such as fiberglass or cellular plastics, forming hybrid thermal assemblies. These materials function by reducing radiative heat transfer, thereby limiting heat gain in hot climates and mitigating heat loss in colder regions. Typically, RIs consist of aluminum foil or similar reflective surfaces positioned adjacent to air cavities. For over a century, these insulation systems have been employed to suppress thermal radiation within enclosed airspaces in building components (IEA, 1987). Presently, RI is integrated into a range of architectural elements, including walls, roofs, insulating glass units in fenestration applications (such as windows, curtain walls, and skylights), as well as within floor joist spaces and metal structures (CMHC, 2004).

A significant body of computational and experimental research has explored the thermal performance of enclosed spaces featuring low-emittance surfaces. For instance, Fricker and Yarbrough (2011) evaluated four computational methods for estimating the thermal resistance of reflective airspaces. Saber et al. (2022) utilized a numerical model to develop practical correlations for predicting thermal resistance in different configurations, including: (a) vertical enclosed airspaces with horizontal heat flow; (b) horizontal airspaces with both upward and downward heat flow; (c) 30° and 45° inclined airspaces with both upward and downward heat flow. Moreover, this model contributed to the development of the Airspace Reflective Tool (ART), which is designed to calculate the *R*-values of airspaces across various building applications (Saber et al., 2024).

Steel-framed wall systems, which are the central focus of this study, require precise calculations to determine their U-factors for compliance with building codes. Three primary methods are available for this purpose for steel-framed systems incorporating mass insulation. One widely used approach, incorporated into the 2018 International Energy Conservation Code (IECC) (IECC, 2018), employs a series path technique to estimate thermal bridging effects in parallel paths by applying correction factors. However, this method is limited in scope as it only covers ten specific construction configurations listed in a predefined lookup table. An alternative approach, presented in the 2017 ASHRAE Handbook of Fundamentals (HOF) (ASHRAE, 2017), is specifically designed for nominal 2 inch × 4 inch (measuring 38.1 mm × 88.9 mm) and 2 inch × 6 inch (measuring 38.1 mm × 139.7 mm) wall assemblies, making it unsuitable for a broader range of steel-framed constructions. Given these limitations, accurately determining the thermal resistance (*R*-values) of various steel-framed wall assemblies requires experimental testing or advanced simulations. One standardized experimental method is guarded hot box (GHB) testing, conducted in accordance with ASTM C1363 (ASTM, 2020b), which provides reliable thermal performance data under controlled conditions. Additionally, validated numerical modeling offers an approach for predicting the thermal behavior of steel-framed walls across different design scenarios, enabling a more comprehensive assessment of their insulating performance.

RI materials, including aluminum foils and specialized coatings, have emerged as viable solutions for enhancing the thermal performance of building envelope components. A critical characteristic of these materials is their low emittance, which reduces radiative heat transfer. The emittance of RI is typically measured using the ASTM C1371 test method (ASTM, 2020a), ensuring standardized assessment of its thermal properties. In this study, RI materials are integrated within the cavities of steel-framed

walls, positioned between different structural layers to optimize thermal resistance. While conventional insulation methods, such as fiberglass batts, loose-fill insulation, and spray foam, have been extensively studied, the thermal behavior of RIs in steel-framed construction remains less thoroughly documented. In 2015, the American Iron and Steel Institute (AISI) introduced a comprehensive Design Guide, titled "Thermal Design and Code Compliance for Cold-Formed Steel Walls," which provides U-values (reciprocals of *R*-values) for steel-framed wall assemblies containing fiberglass insulation (American Iron and Steel Institute, 2015). However, this guide does not include data or design considerations for RI in steel-framed walls, highlighting a critical gap in existing resources.

Unlike mass insulation, which primarily relies on conduction to reduce heat transfer, RI operates by minimizing radiative heat exchange within enclosed airspaces. The distinct configuration and working principles of RI necessitate targeted research to evaluate their performance in steel-framed wall assemblies. Consequently, there is a strong need for experimental and computational studies to generate reliable performance data, which can inform design guidelines and increase code compliance for buildings utilizing RI in steel structures.

Objectives

The goal of this study is to examine the thermal behavior of steel-framed wall assemblies that incorporate a reflective insulation system (RIS) and hybrid systems, which combine RI with conventional mass insulation. To ensure that the outcomes of this study are broadly applicable, a wide variety of cases have been considered. These cases differ in fundamental ways, including whether reflective insulation is present (i.e., emittance <0.2) or absent (i.e., emittance = 0.9), whether cavities are partially or completely filled with conventional mass insulation, and whether low-e or high-e surfaces are used. By systematically varying these parameters, the study isolates their individual and combined effects on the effective thermal resistance (R_{eff}) of steel-framed systems. In addition, this broad coverage ensures that each case conveys unique information, while also generating a comprehensive dataset that can inform both scientific understanding and practical design guidelines. Using a previously developed and validated three-dimensional numerical model, this research investigates the impact of thermal bridging, natural convection, and radiative heat transfer within these assemblies. The specific objectives include:

1. Evaluating the performance of RISs:
   - Assess the contribution of RI in reducing heat transfer within steel-framed wall systems.
   - Quantify the effect of different RIS configurations and emittance values on the effective thermal resistance (R_{eff}) of the assembly.
   - Compare the thermal performance of RIS against conventional steel-framed wall assemblies without RI.
2. Investigating hybrid systems incorporating reflective and mass insulation:
   - Analyze the thermal properties of hybrid systems that integrate RI with different types and quantities of conventional insulation materials.
   - Determine the extent to which hybrid systems improve the thermal resistance of steel-framed wall assemblies compared to a standalone RIS and conventional insulation.
   - Identify optimal configurations of reflective and mass insulation for increased thermal performance.
3. Examining the impact of thermal bridging in steel-framed wall assemblies:
   - Investigate how steel framing components (studs, top tracks, and bottom tracks) contribute to thermal bridging and overall heat loss.
   - Develop a methodology for separating the effects of thermal bridging from the numerical simulation results to determine the thermal resistance of wall cavities for RIS and hybrid systems.
   - Assess the influence of different thermal emittance values on RISs and hybrid systems on energy performance.
4. Providing design recommendations for RI in steel-framed structures:
   - Generate data to support the inclusion of RISs and hybrid systems in building codes and design guidelines, such as the 2015 Edition of Thermal Design and Code Compliance for Cold-Formed Steel Walls.
   - Offer recommendations to architects, engineers, and designers on optimal RIS configurations to maximize energy efficiency.
   - Consider the full range of surface emittance (0–0.9) in order to address potential long-term factors affecting RI performance, such as dust accumulation and moisture condensation, that can increase the emittance, to ensure practical applicability of the findings.

By achieving these objectives, this study aims to provide a comprehensive understanding of the role of RI in steel-framed building design and contribute to more effective and energy-efficient thermal insulation strategies. To achieve these objectives, an array of numerical simulations is conducted to generate *R*-values for steel-framed systems without and with mass insulation of various types and quantities, and without and with RI of different emittances over the range of 0.0–0.9. For wall applications, the array simulations are conducted for horizontal heat flow (see Figure 1). A brief description of the model used in this study is provided next.

Brief model descriptions and validations

The previously developed numerical model has been employed in various research investigations to assess both the thermal and moisture performance of building envelope components incorporating different types of insulation materials, including reflective insulation systems. This model is capable of handling both steady-state and transient conditions by simultaneously solving two-dimensional and three-dimensional governing equations. These equations encompass the moisture transport equation, the energy

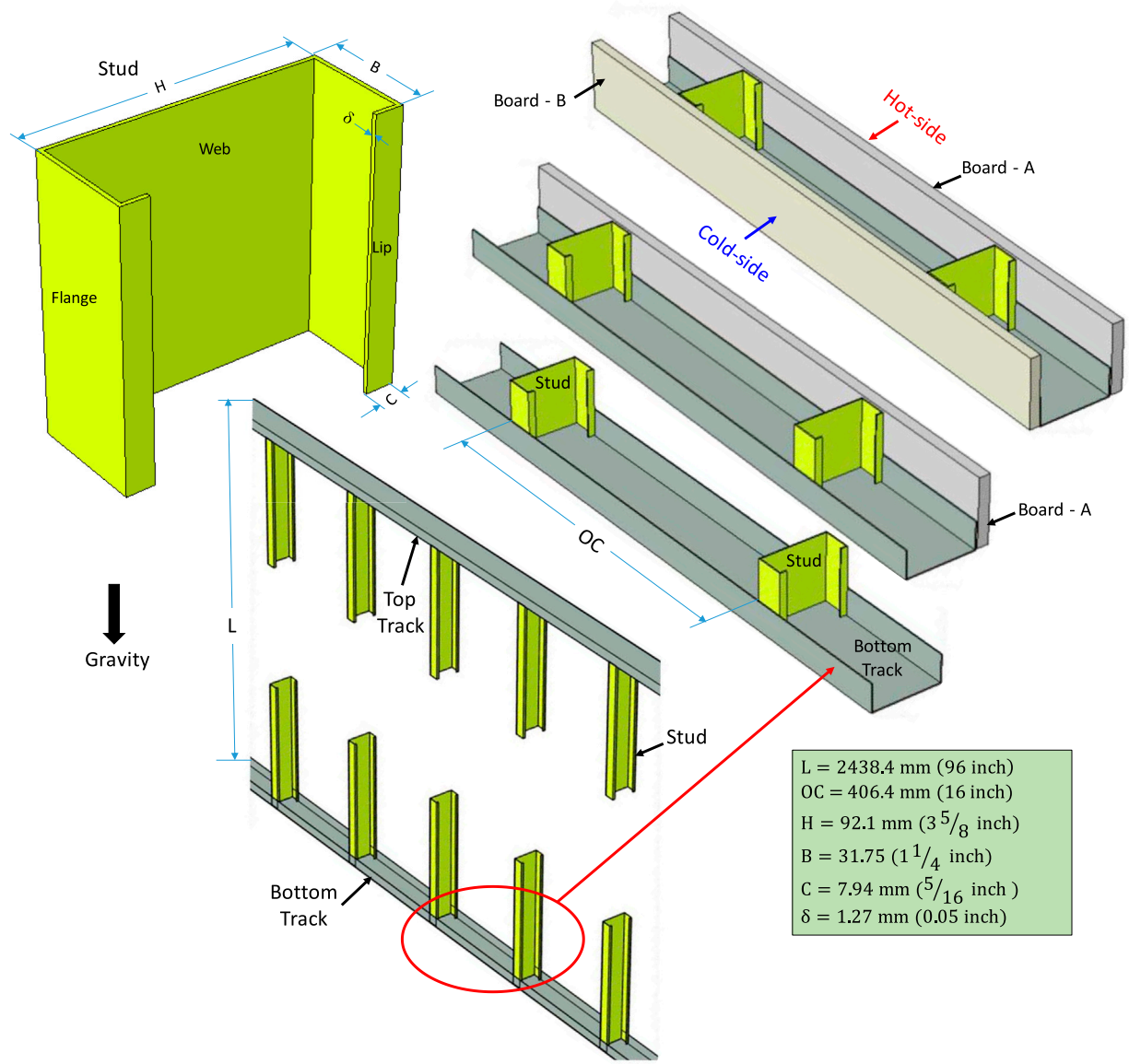

FIGURE 1
Schematic of a steel-framed wall.

conservation equation, radiative heat transfer between surfaces within enclosed airspaces, radiation exchange between exterior surfaces and the ambient environment, as well as the momentum equation governing air movement within ventilated or non-ventilated airspace layers. The mathematical formulations for these equations are detailed in Saber and Yarbrough (2023a), Saber and Yarbrough (2021), and Saber et al. (2011). In the present study, the numerical model is specifically applied to evaluate the thermal resistance characteristics of steel-framed wall assemblies under steady-state thermal conditions, with no consideration of moisture transport.

Three standard testing methods are commonly utilized in building-related applications, including those addressed in this study:

a. Guarded hot box (GHB) as specified by ASTM C236 (ASTM, 1953),
b. Guarded hot plate (GHP) and heat flow meter (HFM) as outlined in ASTM C518 (ASTM, 2003), and
c. GHB following ASTM C1363 (ASTM, 2020b).

The model was validated using experimental data obtained through the test methods outlined earlier. As documented in Saber and Yarbrough (2021), the predicted thermal resistances were evaluated against data from HRP 32 (Robinson et al., 1954), which were measured utilizing a guarded hot box in accordance with ASTM C236 (ASTM, 1953). The comparisons encompassed vertical and horizontal single- and double-enclosed airspaces exposed to various heat flow directions (horizontal for wall applications, and

upward and downward for roof applications). The test data involved a single-enclosed airspace with a thickness of 88.9 mm and a length of 812.8 mm, as well as a double-enclosed airspace with two equal layers, each 44.45 mm thick and 812.8 mm in length. The tests were accomplished at an average temperature of 23.9 °C with a temperature difference of 16.6 °C (T_H = 32.2 °C, T_L = 15.6 °C). For a wide range of emittance values, the thermal resistances predicted by the model showed agreement with the data from HRP 32 for both single- and double-enclosed airspaces under various heat flow directions, with discrepancies within ±5%.

The model was validated using experimental data from sample stacks containing enclosed airspaces. Each test specimen consisted of two expanded polystyrene (EPS) layers, each measuring 304.8 mm × 304 mm × 25.4 mm, with an enclosed airspace (203.2 mm × 203.2 mm × 25.4 mm) located at the center of a third EPS layer of the same size. This central EPS layer was positioned between the EPS lower layer and the EPS upper layer. In the first sample stack, aluminum foil was applied to the bottom surface of the upper EPS layer, while the second sample stack did not include aluminum foil. The sample stacks were tested horizontally under heat flowing up using a heat flow meter, following the procedures outlined in ASTM C518 (ASTM, 2003). The heat fluxes calculated for the cold surface and hot surfaces of sample stacks showed agreement with the experimental results, with discrepancies within ±1.0% (Saber, 2012).

The thermal resistance of a full-scale wood-framed wall assembly, measuring 2,438.4 mm by 2,438.4 mm, was experimentally determined using a GHB apparatus in accordance with ASTM C1363 (ASTM, 2020b). The results obtained from the test were compared with the results predicted by the model. The tested wall assembly was constructed using nominal 2 inch × 6 inch (measuring 38.1 mm × 139.7 mm) spruce wood framing members, spaced at 406.4- mm intervals from center to center. The framing configuration included double top plates and a single bottom plate. Fiberglass batt insulation was installed within the stud cavities, held securely in place through friction fitting to eliminate air gaps. A layer of foil-faced fiberboard was installed on the interior side of the wall framing, with the reflective foil surface oriented toward a furred airspace assembly (FAA). The FAA was constructed using horizontal wood furring strips, each measuring 19.05 mm by 64 mm, positioned with 406.4 mm center-to-center spacing. This furred airspace was enclosed by 12.7-mm-thick gypsum board, forming a defined air cavity that contributed to the overall thermal performance of the wall system. The exterior side of the wall assembly was clad with 11-mm-thick wood fiberboard, providing additional structural support and insulation. The comparison between the model predictions and the experimental results demonstrated a high level of agreement with the numerically calculated thermal resistance, differing from the measured value by only 1.2% (Saber et al., 2011). This agreement validates the reliability of the numerical model in simulating the thermal behavior of a full-scale wall assembly incorporating RI. The present study extends the application of the model to evaluate the thermal performance of full-scale steel-framed wall systems containing both RI and mass insulation. The analysis considers a broad spectrum of surface emittance values, allowing for a comprehensive assessment of the impact of radiative heat transfer characteristics on overall thermal resistance.

Description of a steel-framed wall

Three-dimensional simulations were carried out using the previously described model to analyze the performance of a steel-framed wall, as depicted in Figure 1. The figure illustrates a full-scale wall system with dimensions of 2,438.4 mm × 2,438.4 mm (W × H), comprising C-shaped steel studs spaced 406.4 mm apart (center to center) and steel tracks positioned at the top and bottom. The C-shaped studs have a thickness of 1.27 mm (T), a web length of 92.1 mm (D) representing the cavity depth, a flange length of 31.75 mm (B), and a lip length of 7.94 mm (C). Two boards are installed on the steel-framed wall: Board-A is fastened to the steel tracks on the hot side, while Board-B is secured to the steel tracks on the cold side. Due to repeatability, the numerical simulations were conducted for one module. This module is shown by the black-dashed box in Figure 2 (showing a horizontal cut passing through the steel studs) and Figure 3 (showing a horizontal cut passing through the mid-height of the steel rack). 3-D surface-to-surface radiations occur on all inner surfaces of the racks, studs, Board-A, and Board-B. Figure 2 shows that RI with emittance ε_1 is applied on the inner surface of Board-A. The emittance of the other surfaces that are facing airspaces is given by ε_2 (see Figures 2, 3). In this study, numerical simulations were conducted for two cases:

a. Case A, in which the RI on the inner surface of Board-A facing airspace has the full range of the emittance ε_1 (0–0.9), and the emittance ε_2 for all other surfaces facing airspaces is 0.9 (ASHRAE, 2017) (Figure 2).
b. Case B, in which the thermal emittance of all surfaces facing airspaces ($\varepsilon_1 = \varepsilon_2$) has a wide range of 0–0.9 (Figures 2, 3).

Cases A and B pertain to steel-framed wall assemblies that incorporate a reflective insulation system (RIS). This research focuses on evaluating the thermal performance of these systems, specifically in scenarios without mass insulation in the wall cavity (the air gap between the steel studs), and when the wall cavity is partially occupied by mass insulation. In the first part of this study, a representative case was examined in which a 50.8-mm-thick layer of mass insulation with a thermal conductivity of 0.04 W/(m·K) was integrated into the wall cavity. This thermal conductivity value closely aligns with that of conventional fiberglass batt insulation. Throughout the article, the unit W/(m·K) is used for the thermal conductivity of mass insulation and will not be explicitly stated unless otherwise specified.

The simulations were carried out for both Cases A and B under conditions where the mass insulation was positioned against the inner surface of Board-B, as depicted in Figures 2b,c, 3b,c. The steel-framed wall assemblies for Cases A and B, which combine reflective and mass insulation, are referred to as "Hybrid Systems" in this research. In the second part of this study, simulations were conducted to assess the energy performance of Hybrid Systems when the wall cavities were partially and fully occupied with various types of mass thermal insulation available in the market.

For reflective insulation in building applications, the ASTM C1224 standard test method outlines a methodology for separating the effects of framing thermal bridges from the measured effective thermal resistance of the assembly. This approach enables the determination of the thermal resistance provided solely by the RI

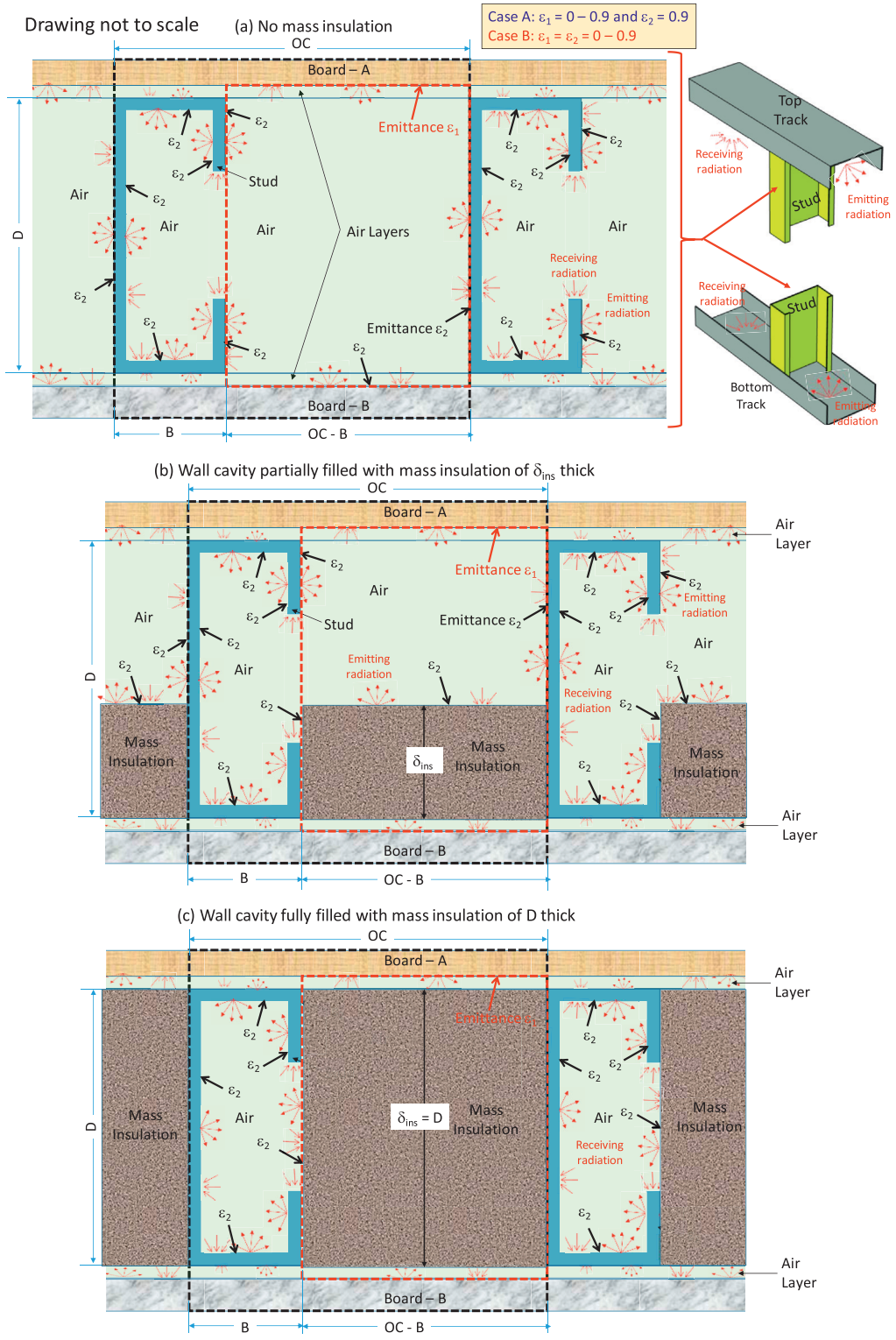

FIGURE 2
Schematic of a horizontal cut passing the wall mid height for the cases: **(a)** no mass insulation, **(b)** wall cavity partially with mass insulation, and **(c)** wall cavity fully filled with mass insulation.

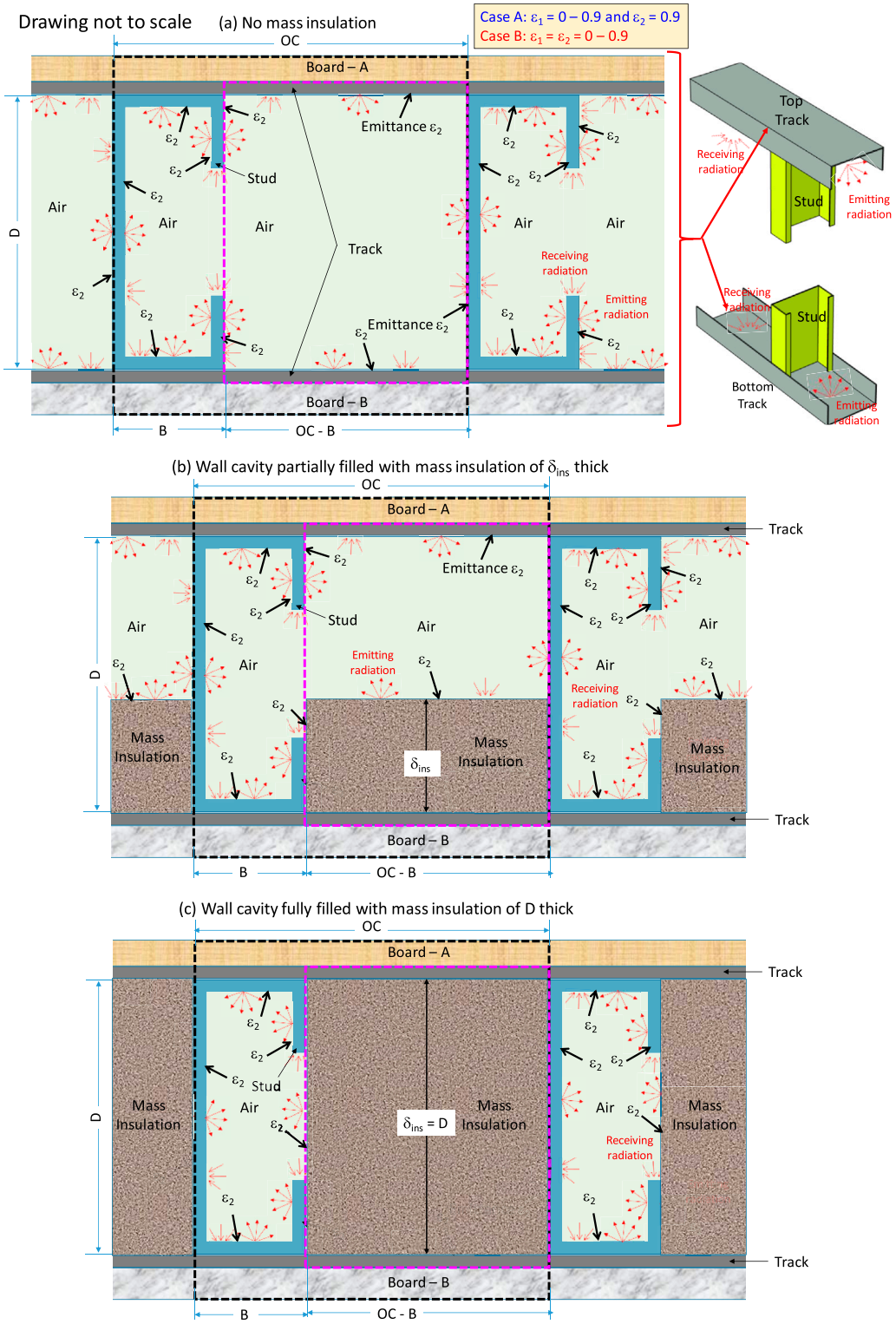

FIGURE 3
Schematic of a horizontal cut passing the steel racks for the cases: **(a)** no mass insulation, **(b)** wall cavity partially with mass insulation, and **(c)** wall cavity fully filled with mass insulation.

(ASTM, 2021). Similarly, in this study, the impact of the framing thermal bridges was accounted for and then separated to evaluate the thermal resistance of the RI within steel-framed assemblies for both the RIS and the hybrid system configurations. To follow the same ASTM C1224 methodology, the simulation results were analyzed to evaluate the thermal resistances of steel-framed wall systems using the procedure described next.

Procedure for analyzing numerical results to determine thermal resistances of steel-framed systems

This research aims to evaluate the thermal resistances (*R*-values) of steel-framed wall systems, requiring calculations under steady-state conditions. Thus, the numerical model described earlier was used to perform steady-state simulations for steel-framed systems with and without RI, as well as with and without mass insulation. Thereafter, the numerical results for both local heat fluxes and temperatures are used to evaluate the surface-to-surface effective thermal resistances of wall assemblies, called R_{eff}, as follows:

$$R_{eff} = \frac{\Delta T}{q_{avg}}, \textit{where} \tag{1}$$

$$\Delta T = \frac{1}{A_H}\int_{A_H} T \cdot dA_H - \frac{1}{A_C}\int_{A_C} T \cdot dA_C, \textit{and} \tag{2}$$

$$q_{avg,H} = \frac{1}{A_H}\int_{A_H} q_{n,H} \cdot dA_H \textit{ and } q_{avg,C} = \frac{1}{A_C}\int_{A_C} q_{n,C} \cdot dA_C \tag{3}$$

In this study, the values of R_{eff} in Equation 1 are provided for the steel-framed system without the thermal resistance of Board-A (R_{b-A}) and the thermal resistance of Board-B (R_{b-B}). Thus, the value of the total effective thermal resistance of the wall system ($R_{eff,tot}$) is simply equal to the sum of R_{eff}, R_{b-A} and R_{b-B}. The value of ΔT in Equation 2 is the difference in temperatures between the hot surface (i.e., at the Board-A–top and bottom rack interface) and the cold surface (i.e., at the Board-B–top and bottom racks interface) of the building assembly. In Equations 2 and 3, A_C is the area of the cold surface, and A_H is the area of the hot surface. For a full module in the wall assembly (see the dashed-black box in Figure 2) and using the dimensions shown in Figure 1, $A_H = A_C = 0.991\ m^2$.

In Equation 3, $q_{n,H}$ and $q_{n,C}$, respectively, are the local normal heat flux on the module hot surface and cold surface, and $q_{avg,H}$ and $q_{avg,C}$ are the corresponding average normal heat fluxes on a hot surface and a cold surface. Due to energy conservation, the total heat rate on the hot-side module (i.e., $\int_{A_H} q_{n,H} \cdot dA_H$) must equal the total heat rate on the cold-side module (i.e., $\int_{A_C} q_{n,C} \cdot dA_C$). When the area of the hot side (A_H) is equal to the area of the cold side (A_C), which is the case of this study, the average normal heat flux (q_{avg}) in Equation 1 that is needed to determine R_{eff} is equal to $q_{avg,H}$ or $q_{avg,C}$. However, for a building assembly in which $A_H \neq A_C$ (i.e., $q_{avg,H} \neq q_{avg,C}$), R_{eff}, based on the hot side, is calculated from Equation 1 with $q_{avg} = q_{avg,H}$, whereas R_{eff}, based on the cold side, is evaluated with $q_{avg} = q_{avg,C}$.

As mentioned earlier, several previous studies have shown that thermal bridges caused by a metal frame can significantly affect the overall performance of the metal-framed systems. To show the influence of the thermal bridges in this study, the thermal resistance of the steel frame, called R_{Fra}, is determined using the numerical results for both local heat fluxes and temperatures in the steel-framed components, namely:

a. Steel studs including the air filling the C-channels, the thin air layer of B wide, T thick, and (L − 2B) long (L = 2,438.4 mm, B = 31.75 mm, and T = 1.27 mm, see Figures 1, 2) between the studs and Board-A, and that between the studs and Board-B.
b. Top and bottom steel racks, including the air filling the racks for the RIS, and air and mass thermal insulation filling the racks for the hybrid system.

For the steel frame, the area of the hot surface ($A_{H,Fra}$) and the area of cold surface ($A_{C,Fra}$) are shown in blue in Figure 4.

The thermal resistance of a steel frame R_{Fra} is determined as

$$R_{Fra} = \Delta T_{Fra} / q_{avg,Fra} \tag{4}$$

$$\Delta T_{Fra} = \frac{1}{A_{H,Fra}}\int_{A_{H,Fra}} T \cdot dA_{H,Fra} - \frac{1}{A_{C,Fra}}\int_{A_{C,Fra}} T \cdot dA_{C,Fra} \tag{5}$$

$$q_{avg,Fra,H} = \frac{1}{A_{H,Fra}}\int_{A_{H,Fra}} q_{n,H} \cdot dA_{H,Fra}, \textit{and} \tag{6}$$

$$q_{avg,Fra,C} = \frac{1}{A_{C,Fra}}\int_{A_{C,Fra}} q_{n,C} \cdot dA_{C,Fra} \tag{7}$$

As per the dimensions in Figure 1 for a steel-framed wall system, $A_{C,Fra} = A_{H,Fra} = 0.101\ m^2$. Additionally, the ratio of the steel framing exterior surface area (studs, top rack, and bottom rack, $A_{C,Fra}$ or $A_{H,Fra}$) to the total exterior surface area (A_C or A_H), called the "framing-to-wall surface area ratio, ξ," is equal to 10.2% in this study. The ΔT_{Fra} in Equation (5) is the difference of the temperatures between the hot side and the cold side of the framing. In Equations 6 and 7, respectively, $q_{n,H}$ and $q_{n,C}$ are the local normal heat fluxes on the hot side and the cold side of the framing, whereas the corresponding average normal heat fluxes on the hot side and the cold side are $q_{avg,Fra,H}$ and $q_{avg,Fra,C}$.

Note that the transport phenomena of all modes of heat transfer (convection, conduction, and radiation), as well as airflow inside the steel framing system, occur in three-dimensional space. The amount of heat entering the framing at the hot side (i.e., $\int_{A_{H,Fra}} q_{n,H} \cdot dA_{H,Fra}$) could be different from that leaving the framing at the cold side (i.e., $\int_{A_{C,Fra}} q_{n,C} \cdot dA_{C,Fra}$). Consequently, the average normal heat flux on the framing hot side ($q_{avg,Fra,H}$) could also be different than the average normal heat flux on cold-side framing ($q_{avg,Fra,C}$). Using Equation 4, the calculated values for R_{Fra} are obtained when: (a) $q_{avg,Fra}$ is based on the framing hot side (i.e., $q_{avg,Fra} = q_{avg,Fra,H}$), and (b) $q_{avg,Fra}$ is based on cold-side framing (i.e., $q_{avg,Fra} = q_{avg,Fra,C}$). As will be shown later, the obtained value for R_{Fra} based on the hot-side framing is not equal to that based on the cold-side framing.

In this study, the performance of the steel-framed wall is reported in terms of three thermal resistances: (a) the effective

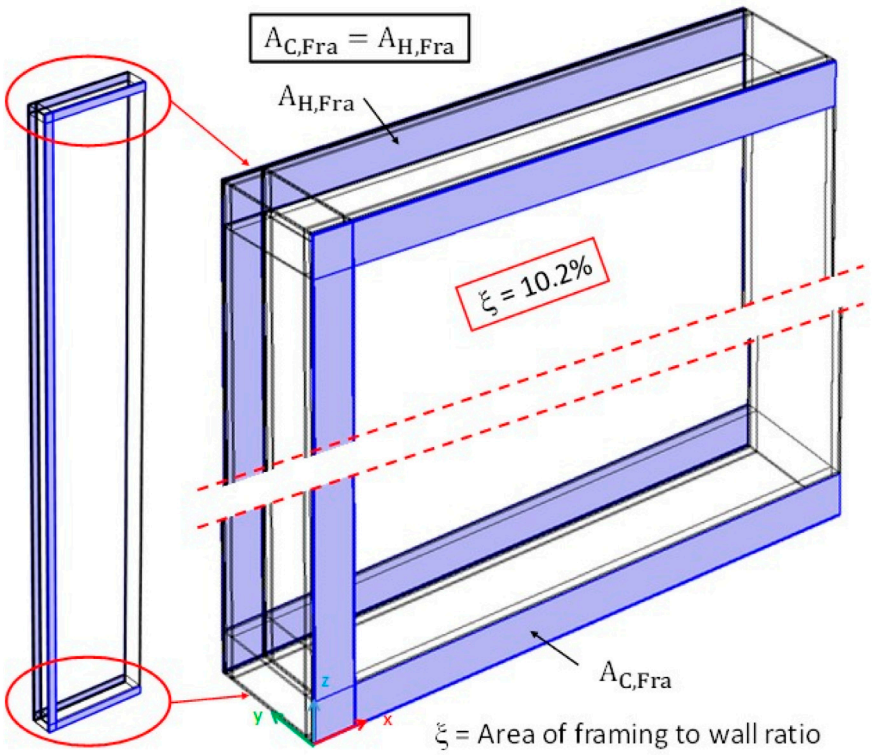

FIGURE 4
Schematic showing ξ-value: the ratio of framing exterior surface area (studs, top rack, and bottom rack) to the total exterior surface area (10.2% in this study).

resistance (R_{eff}, see Equations 1–3), (b) resistance of the steel frame (R_{Fra}, see Equations 4–6), and (c) wall cavity resistance (R_{Cav}). For each module of the steel-framed system, the wall cavity is represented by the red-dashed box in Figure 2. Inside this box, the wall cavity is the part of the simulated module, which is a rectangular prism enclosed by a steel stud at the right side, a steel stud at the left side, a steel rack at the top, a steel rack at the bottom, Board-B at the front, and Board-A at the back (see Figures 1, 2). The materials inside the wall cavity include:

a. The thin air layer of (OC – B) wide (374.65 mm) and T thick (1.27 mm) located between Board-A and the main wall cavity, and that between Board-B and the main wall cavity (see Figure 2). In this study, the main wall cavity between the studs is (OC – B) wide (374.65 mm) and D thick (92.1 mm).
b. The rectangular prism part of the main wall cavity above the bottom steel rack and below the top steel rack when this part is filled by air for the RIS, and air and mass thermal insulation for the hybrid systems. It is important to point out that the rectangular prism parts inside the top and bottom steel racks are already included in the steel frame, as indicated earlier.

As per the information provided above, the wall cavity thermal resistance, called R_{Cav}, is determined as

$$R_{Cav} = \Delta T_{Cav} / q_{avg,Cav} \quad (8)$$

$$\Delta T_{Cav} = \frac{1}{A_{H,Cav}} \int_{A_{H,Cav}} T \cdot dA_{H,Cav} - \frac{1}{A_{C,Cav}} \int_{A_{C,Cav}} T \cdot dA_{C,Cav} \quad (9)$$

$$q_{avg,Cav,H} = \frac{1}{A_{H,Cav}} \int_{A_{H,Cav}} q_{n,H} \cdot dA_{H,Cav}, \text{ and} \quad (10)$$

$$q_{avg,Cav,C} = \frac{1}{A_{C,Cav}} \int_{A_{C,Cav}} q_{n,C} \cdot dA_{C,Cav} \quad (11)$$

In Equations 9–11 and as per the dimensions shown in Figure 1, the exterior surface areas of the wall cavity, described above, for the simulated module on the hot side ($A_{H,Cav}$) is equal to that on the cold side ($A_{C,Cav}$), $A_{H,Cav} = A_{C,Cav} = 0.890\ m^2$. The ΔT_{Cav} in Equation 9 is the temperature difference between the hot side and the cold side of the wall cavity. In Equations 10 and 11, respectively, $q_{n,H}$ and $q_{n,C}$ are the local normal heat fluxes on the hot side and the cold side of the wall cavity. In addition, $q_{avg,Cav,H}$ and $q_{avg,Cav,C}$ in Equations 10 and 11 are the corresponding average normal heat fluxes on the hot and cold sides of the wall cavity. Similar to the steel frame, due to the three-dimensional phenomena for the air and heat transport, the amount of heat entering the wall cavity at the hot side ($\int_{A_{H,Cav}} q_{n,H} \cdot dA_{H,Fra}$) could be different from that leaving the wall cavity at the cold side ($\int_{A_{C,Cav}} q_{n,C} \cdot dA_{C,Cav}$). Even though $A_{C,Cav}$ is

equal to $A_{H,Cav}$, the calculated value for the average normal heat flux on the cavity hot side ($q_{avg,Cav,H}$) could be different than that on the cold side ($q_{avg,Cav,C}$). Therefore, the value calculated for the wall cavity, R_{Cav}, using Equation 8 is obtained based on: (a) the hot side, where $q_{avg,Cav} = q_{avg,Cav,H}$, and (b) the cold side, where $q_{avg,Cav} = q_{avg,Cav,C}$.

This study examined the energy performance of steel-framed assemblies incorporating reflective insulation under the standard labeling conditions (average temperature of 23.9 ˚C and temperature difference of 16.6 ˚C). Thus, the numerical simulations for steel-framed wall systems with and without RI, as well as with and without thermal mass insulation, were performed under the following assumptions: (a) an isothermal condition on the hot side of T_H of 32.2 ˚C at the interface between Board-A and the top and bottom steel racks, and (b) an isothermal condition on the cold side of a T_C of 15.6 ˚C at the interface between Board-B and the top and bottom steel racks. Thus, the values of ΔT in Equation 1, ΔT_{Fra} in Equation 4, and ΔT_{Cav} in Equation 8 are equal, which are 16.6 ˚C. A prior study was performed to investigate whether assuming isothermal conditions on both the hot and cold surfaces was appropriate for calculating and reporting the *R*-values of reflective enclosed airspaces, as well as reflective enclosed airspaces within building assemblies used in various building applications (Saber and Yarbrough, 2023b). The results of that study showed that using isothermal conditions on the hot surface and cold surface affected the predicted *R*-values by only ±3% (Saber and Yarbrough, 2023b).

Both thermal resistances for the steel frame (R_{Fra}) and the wall cavity (R_{Cav}) are in parallel. After determining: (a) the framing-to-wall surface area ratio, ξ (10.2% in this study, see Figure 4), (b) the value of R_{Fra} using Equation 4, and (c) the value of R_{Cav} using Equation 8, the effective surface-to-surface thermal resistance of a steel-framed wall system (R_{eff}) can then be determined as

$$R_{eff} = 1 \Big/ \left[\frac{\xi}{R_{Fra}} + \frac{(1-\xi)}{R_{Cav}} \right] \tag{12}$$

In Equation 12, the R_{eff} should be determined when both R_{Fra} and R_{Cav} are evaluated based on the hot side, or when both R_{Fra} and R_{Cav} are evaluated based on the cold side. Note that the values for R_{Fra} (Equation 4) and R_{Cav} (Equation 8) are evaluated from the obtained numerical results due to fully coupling the three-dimensional transport phenomena of heat transfer modes (convection, conduction, and radiation) as well as airflow inside the steel-framed wall system. As such, the value obtained for R_{eff} from Equation 1 must be the same as that obtained from Equation 12. Finally, it is important to emphasize that all thermal resistances presented in this article represent surface-to-surface values, excluding the contributions of thermal resistances associated with surface film coefficients on the exterior surfaces.

Results and discussion

This section presents the findings of three-dimensional numerical simulations conducted for steel-framed systems subjected to an average temperature of 23.9 ˚C and a temperature differential of 16.6 ˚C, which are standard conditions used for labeling reflective insulation products (i.e., the hot-side temperature of 32.2 ˚C and the cold-side temperature of 15.6 ˚C). The analysis focuses on two primary configurations: reflective insulation systems (RISs), where the wall cavity lacks any mass thermal insulation, and hybrid systems, which incorporate both RI and mass thermal insulation within the cavity. The discussion provides comprehensive insights into several key aspects. First, air flow patterns within steel-framed systems are illustrated to highlight the heat transfer by natural convection within the steel-framed systems. Second, the thermal resistances of both RISs and hybrid systems are quantified and analyzed for specific scenarios, referred to as Cases A and B. Additionally, the extent to which thermal bridges within steel-framed systems reduce their overall thermal resistance is evaluated. The influence of the type and quantity of mass insulation on the thermal performance of hybrid systems is also examined in detail. Based on the results and interpretations provided, potential areas for future research are identified. These areas aim to advance the understanding of thermal behavior in steel-framed systems and to optimize the design of both RISs and hybrid systems for increasing the energy performance of steel-framed systems.

Airflow in steel-framed systems

The temperature gradient across the steel-framed wall generates buoyancy-driven airflow within the airspaces inside the C-shaped steel studs and the wall cavity between them. This airflow leads to the development of convective loops within these regions. The number and behavior of these convective loops are influenced by the orientation of the steel-framed assembly and the direction of heat transfer through the structure. This study focuses on a vertically oriented steel-framed wall system, which corresponds to a scenario where heat flows horizontally through the assembly. Under these conditions, a single convection loop forms within each airspace of the C-shaped steel studs, while an additional convection loop develops within the wall cavity between the studs. For all numerical simulations conducted in this research, the Rayleigh number values within the airspaces were calculated and found to be significantly below 10^9. This confirms that the airflow remains laminar throughout the airspaces.

For the case of emittances ε_1 of 0.05 and ε_2 of 0.9, Figure 5A shows the vertical velocity distribution, V_z, in a vertical slice passing through the mid-width (x = ½ OC) of the steel-framed wall and in a horizontal slice passing through the mid-height (z = ½ H) of a steel-framed wall. The corresponding result for the resultant velocity, $V_{res} = (V_x^2 + V_y^2 + V_z^2)^{0.5}$, is shown in Figure 5B. As shown in this figure, air moves upward near the hot side at the highest vertical velocity of 361 mm/s (shown by the red color) and moves downward near the cold side at the highest vertical velocity of 360 mm/s (shown by the blue color), whereas the highest V_{res} is 361 mm/s (see Figure 5B). Inside the airspace of the C-shaped stud, specifically in horizontal slices passing through the quarter height (z = ¼ H), the mid-height (z = ½ H), and the three-quarter height (z = ¾ H) of the wall system, the corresponding vertical velocity and resultant velocity distributions of the air are shown in Figures 6A,B, respectively. Figure 6A shows that the highest upward vertical velocity and the highest downward vertical velocity are 289 mm/s and 282 mm/s, respectively, whereas the highest V_{res} is 289 mm/s (Figure 6B).

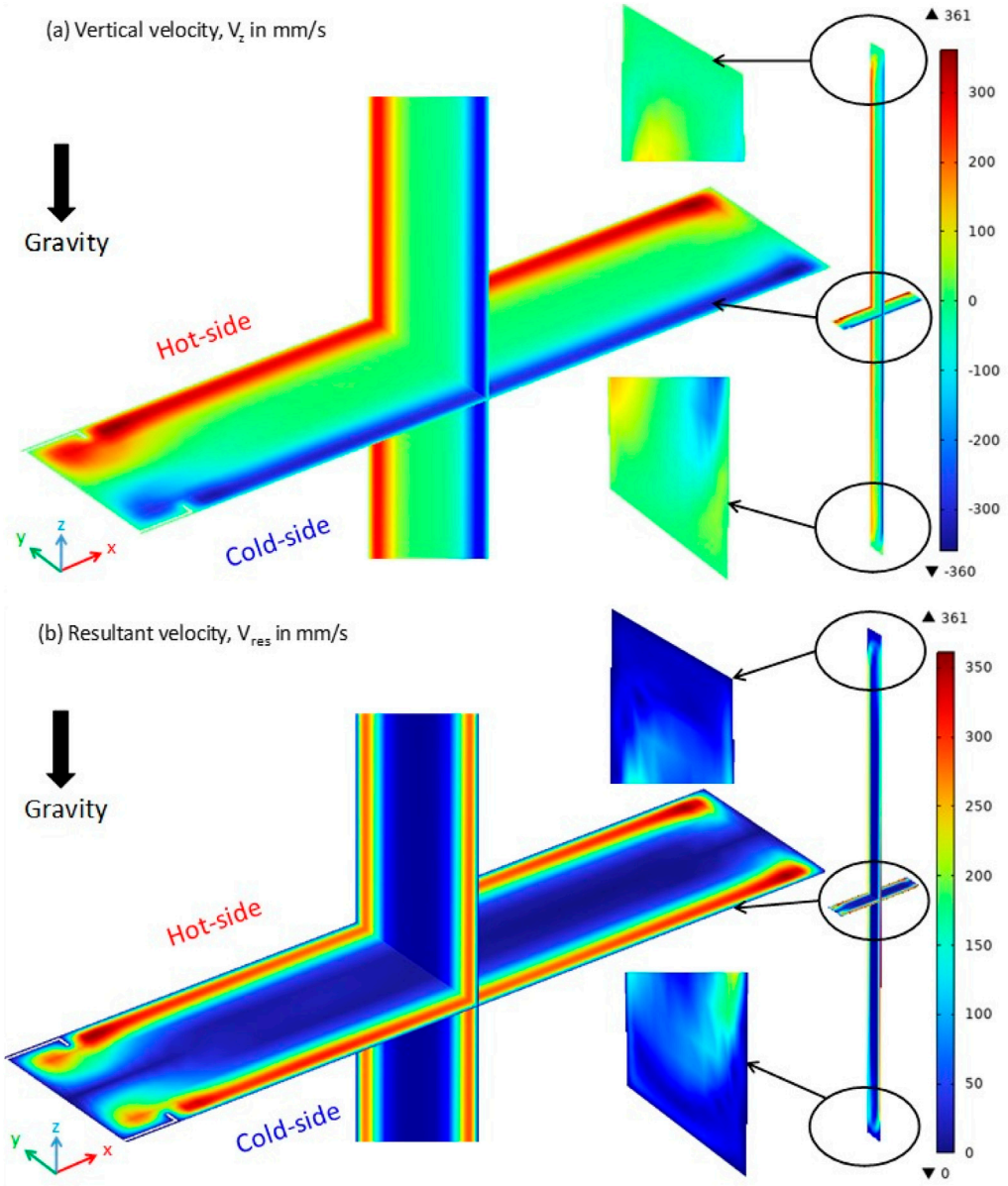

FIGURE 5
For an RIS: **(a)** vertical velocity distribution, and **(b)** resultant velocity distribution in a vertical slice passing through mid-width (x = ½ OC) and in a horizontal slice passing through the half height (z = ½ H) of a steel-framed wall (ε_1 = 0.05, ε_2 = 0.9, T_H = 32.2 °C, T_C = 15.6 °C).

The airspace inside the C-shaped studs is called "AS1," and the airspace in the wall cavity between the studs (see the dashed-red box in Figure 2) is called "AS2." The airflow in AS1 and that in AS2 contribute to the heat transfer by natural convection in the steel-framed assembly. At ε_1 of 0.05 and ε_2 of 0.9 for RIS (no mass insulation in the wall cavity), the volume-weighted average resultant velocity ($V_{res,avg}$) in all airspaces inside the steel-framed assembly (i.e., both AS1 and AS2) is 100.1 mm/s, which corresponds to a Reynolds number (Re) of 839.1. In this study, the Re inside the airspace is defined as: $Re = \rho_a \times V_{res,avg} \times L_c/\mu_a$, and L_c is a characteristic length, which is defined as: $L_c = 4\,V_a/A_a$. In these expressions, ρ_a is the air density (kg/m^3), μ_a is the air dynamic viscosity (Pa·s), V_a is the volume of airspace (m^3), and A_a is the surface area of airspace (m^2). In the AS1, the value of $V_{res,avg}$ is 110.2 mm/s, which corresponds to an Re of 469.8. Whereas the value of $V_{res,avg}$ in the AS2 is 99.4 mm/s (10% lower than that in AS1), which corresponds to an Re of 1,024.4 (approximately twice of that in AS1). A higher Reynolds number leads to an increased convective heat transfer rate. Therefore, the convective heat transfer rate in AS2 would be higher than in AS1.

At an ε_1 of 0.05 and an ε_2 of 0.9 in the hybrid system incorporating mass insulation in the wall cavity with a thickness (δ_{ins}) of 50.8 mm and a thermal conductivity (k_{ins}) of 0.04 W/(m·K), Figures 7A,B, respectively, show the vertical velocity and resultant velocity distributions in a vertical slice passing through mid-width (x = ½ OC) and in a horizontal slice passing through the mid-height (z = ½ H) of the steel-framed wall. As shown in Figure 7A, the highest upward vertical velocity (245 mm/s, in AS2) is 32% lower

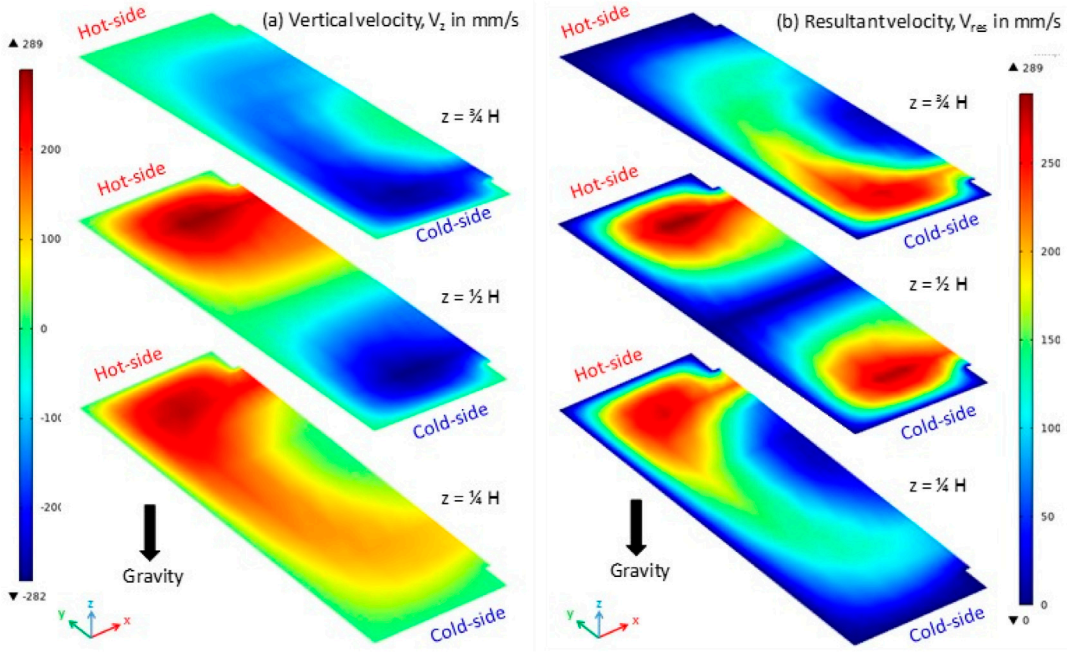

FIGURE 6
For an RIS: **(a)** vertical velocity distribution and **(b)** resultant velocity distribution in horizontal slices passing through the quarter height (z = ¼ H), half height (z = ½ H), and three-quarter height (z = ¾ H) of a steel-framed wall (ε_1 = 0.05, ε_2 = 0.9, T_H = 32.2 °C, T_C = 15.6 °C).

than that for the RIS (361 mm/s, in AS2, Figure 5A); whereas the highest downward vertical velocity (405 mm/s, occurred in AS1) is 13% higher than that for the RIS (360 mm/s, in AS2, Figure 5A). In addition, Figure 7B shows that the highest resultant velocity for the hybrid system (405 mm/s, in the AS1) is 12% higher than that for the RIS (361 mm/s, in AS2, Figure 5B).

Inside the AS1 for the hybrid system, Figures 8A,B, respectively, show the vertical velocity and resultant velocity distributions in three horizontal slices passing through the quarter height (z = ¼ H), mid-height (z = ½ H), and three-quarter height (z = ¾ H) of the wall system. Figure 8A shows that the highest upward vertical velocity for the hybrid system (115 mm/s in the slice at z = ¼ H) is 60% lower than that for the RIS (289 mm/s in the slice at Z = ½ H, Figure 6A). Conversely, the highest downward vertical velocity for the hybrid system (422 mm/s in the slice at z = ¼ H) is 50% higher than that for the RIS (282 mm/s in the slice at z = ½ H, Figure 6A). Figure 8B shows that the highest resultant velocity for the hybrid system (422 mm/s in the slice at z = ¼ H) is 46% higher than that for the RIS (289 mm/s in the slice at z = ½ H, Figure 6B).

For ε_1 of 0.05 and ε_2 of 0.9 in the hybrid system (mass insulation in the wall cavity with δ_{ins} = 50.8 mm and k_{ins} = 0.04 W/(m·K)), $V_{res,avg}$ in all airspaces inside the steel-framed assembly (i.e., both AS1 and AS2) is 90.1 mm/s, which is 10% lower than that for the RIS (100.1 mm/s), where the corresponding Re in the hybrid system (233.0) is 72% lower than that for the RIS (839.1). In the AS1 of the hybrid system, however, the value of $V_{res,avg}$ (132.0 mm/s) is 20% higher than that for the RIS (110.2 mm/s), where the corresponding Re for the hybrid system (550.1) is 17% higher than that for the RIS (469.8). The value of $V_{res,avg}$ in the AS2 for the hybrid system (83.3 mm/s) is 16% lower than that for the RIS (99.4 mm/s), where the corresponding Re for the hybrid system (202.4) is 80% lower than that for the RIS (1,024.4).

Based on the information above and the velocity distributions shown in Figures 5–8, a stronger convection loop is observed in AS2 (i.e., airspace in wall cavity) for the RIS, which leads to a greater reduction in its *R*-value than the hybrid system. In contrast, a stronger convection loop develops in AS1 (i.e., the airspace in the C-shape of the studs) for the hybrid system, leading to a greater reduction in its *R*-value than RIS. The combined effects of natural convection, conduction, and radiation on the effective thermal resistances of the RIS and the hybrid system are discussed next for a broad range of emittance values (ε1 from 0.0 to 0.9).

Thermal resistance of steel-framed systems

The products of RIs typically exhibit emittance values ranging from 0.03 to 0.2. However, the accumulation of dust or condensation of water vapor on their surfaces can lead to an increase in these emittance values. Consequently, this study considers a comprehensive range of emittance ε_1 values, from 0 to 0.9. For the specified values of emittances ε_1 and ε_2 (refer to Figures 2, 3), the impact of air movement on the effective thermal resistance (R_{eff}) of the steel-framed wall, due to convective heat transfer, is influenced by ΔT across the assembly. A larger ΔT leads to faster airflow, resulting in a greater reduction in R_{eff} than a smaller ΔT. The results presented in this study are based on a ΔT of 16.6 °C (T_C = 15.6 °C and T_H = 32.2 °C).

For the simulation Case A, in which emittance ε_2 = 0.9 (ASHRAE, 2017), and the simulation Case B, in which $\varepsilon_1 = \varepsilon_2$, Figure 9 shows the effect of the emittance ε_1 on the effective

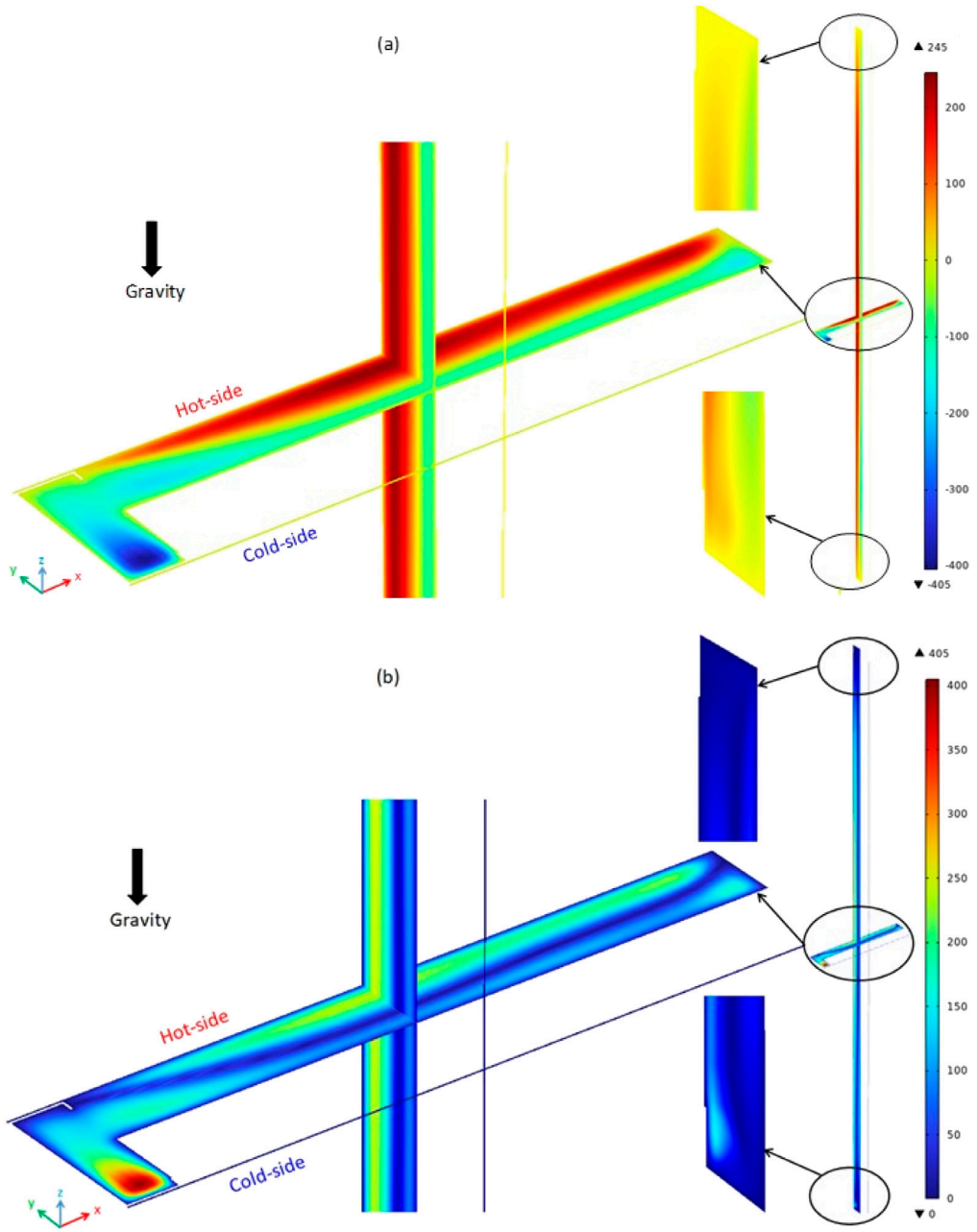

FIGURE 7
For a hybrid system with mass insulation thickness of 50.8 mm at thermal conductivity of 0.04 W/(m·K), **(a)** vertical velocity distribution, and **(b)** resultant velocity distribution in a vertical slice passing through the mid-width (x = ½ OC) and in a horizontal slice passing through the mid-height (z = ½ H) of a steel-framed wall (ε_1 = 0.05, ε_2 = 0.9, T_H = 32.2 °C, T_C = 15.6 °C).

R-value of the steel-framed wall. As shown in Figure 9, ignoring the radiative heat transfer on all inner surfaces facing airspaces inside the steel-framed wall is represented in Case B at $\varepsilon_1 = \varepsilon_2 = 0.0$, for which R_{eff} is equal to 0.421 m^2·K/W. Unless otherwise specified, the unit "m^2·K/W" is used for thermal resistances throughout the article and will not be explicitly mentioned. Ignoring the radiative heat transfer on the inner surface of Board-A facing airspaces between the studs, and simultaneously accounting for radiative heat transfer on all other inner surfaces facing airspaces inside the steel-framed system at $\varepsilon_2 = 0.9$ is represented by Case A at $\varepsilon_1 = 0.0$, for which R_{eff} (0.347) has decreased by 0.074 (i.e., a reduction in R_{eff} of 21.3%) in relation to Case B at $\varepsilon_1 = \varepsilon_2 = 0.0$ (Figure 9). Without using any type of RI in the steel-framed system (i.e., $\varepsilon_1 = \varepsilon_2 = 0.9$), the calculated R_{eff} is 0.153. In this case, ignoring the effect of radiative heat transfer (i.e., $\varepsilon_1 = \varepsilon_2 = 0.0$ at which R_{eff} = 0.421, Figure 9) resulted in overestimating R_{eff} by 175%. Consequently, accurately evaluating the energy performance of steel-framed systems necessitates the precise determination of surface-to-surface radiative heat transfer on all surfaces facing airspaces.

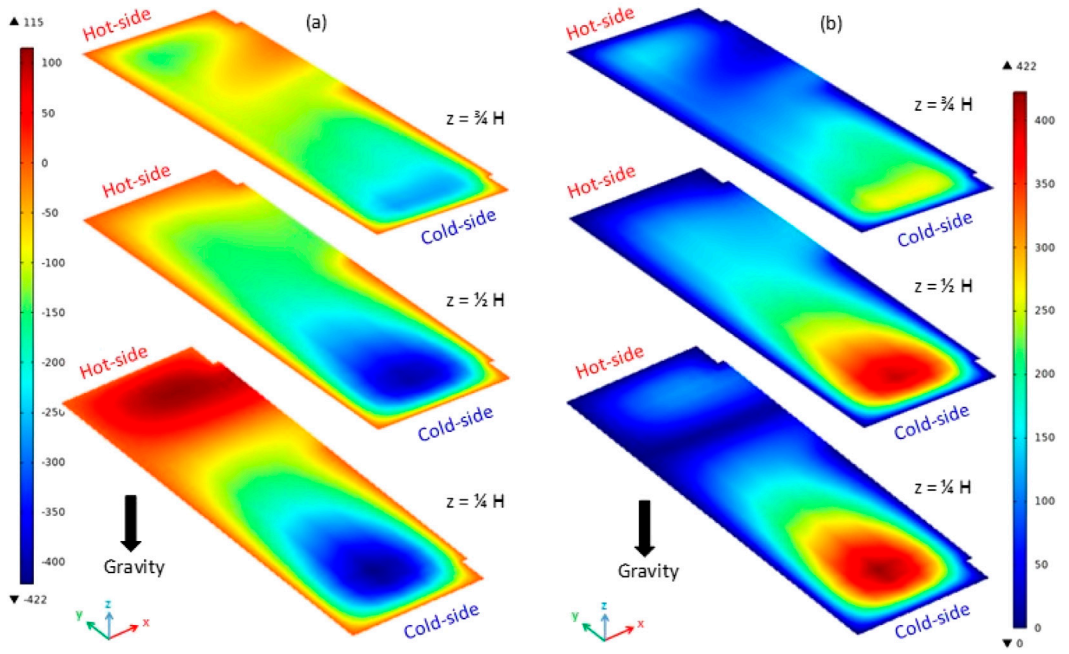

FIGURE 8
For Hybrid System with mass insulation thickness of 50.8 mm at thermal conductivity of 0.04 W/(m·K), **(a)** vertical velocity distribution, and **(b)** resultant velocity distribution in horizontal slices passing through the quarter height (z = ¼ H), mid-height (z = ½ H), and three-quarter height (z = ¾ H) of a steel-framed wall (ε_1 = 0.05, ε_2 = 0.9, T_H = 32.2 °C, T_C = 15.6 °C).

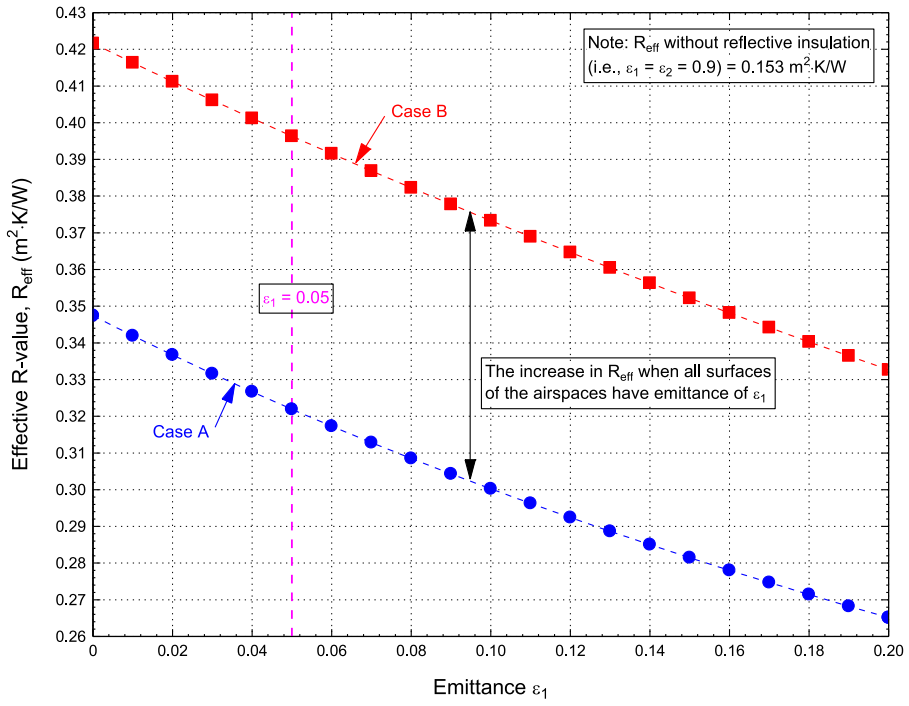

FIGURE 9
For the RIS, the dependence of R_{eff} on the emittance ε_1 for Case A and Case B.

Figure 9 illustrates that incorporating RI with ε_1 = 0.05 on the inner surface of Board-A for Case A leads to a R_{eff} of 0.322, which is approximately 2.1 times greater than the value obtained without RI (ε_1 = 0.9, where R_{eff} = 0.153). Similarly, applying RI with ε_1 = 0.05 to all inner surfaces facing airspaces within the steel-framed wall (Case B, where $\varepsilon_1 = \varepsilon_2$) yields a R_{eff} of 0.396,

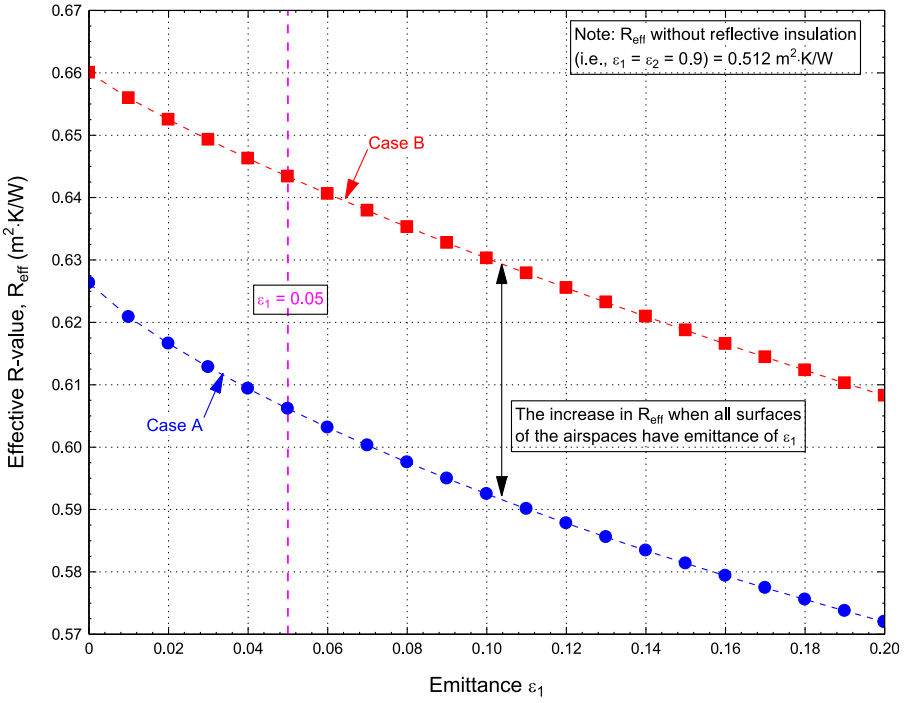

FIGURE 10
For the hybrid system, dependence of R_{eff} on the emittance ε_1 for Case A and Case B [δ_{ins} = 50.8 mm and k_{ins} = 0.04 W/(m·K)].

which is 2.6 times the R_{eff} value without RI ($\varepsilon_1 = 0.9$, $R_{eff} = 0.153$). Furthermore, when RI with $\varepsilon_1 = \varepsilon_2 = 0.05$ is used on all inner surfaces facing airspaces for Case B, the R_{eff} increases by 0.074 (a 23.0% increase) compared to Case A, in which RI ($\varepsilon_1 = 0.05$) is applied only to the inner surface of Board-A (Figure 9). These findings provide valuable insights for building designers in determining whether to adopt the steel-framed system configuration of Case A or Case B.

For both Cases A and Case B, numerical simulations were conducted to evaluate the performance of a steel-framed wall system incorporating a 50.8-mm-thick layer of mass thermal insulation with thermal conductivity (k_{ins}) of 0.04 W/(m·K). The insulation layer was positioned within the wall cavity, situated between the studs, and attached to the inner surface of Board-B (refer to Figures 2, 3). This layer represents a partial filling of the 92.1 mm deep wall cavity, corresponding to an insulation filling ratio (ϕ) of 55.2%. The partial fill reflects a common practical scenario in construction, where cost and material limitations may prevent filling the whole cavity with mass insulation. As discussed previously, the configuration involving only RI within the steel-framed wall is referred to as the RIS, whereas the hybrid system integrates both RI and mass thermal insulation. This combined approach aims to leverage the benefits of both insulation types to increase the thermal resistance. The hybrid system is particularly significant for applications where higher thermal performance is required while maintaining the structural and design characteristics of steel-framed walls. In addition, the inclusion of both RI and mass insulation in the hybrid system offers a pathway to achieve improved energy efficiency and thermal comfort in modern construction.

For the hybrid system, Figure 10 illustrates the relationship between the R_{eff} of the steel-framed wall with mass insulation and the emittance of the RI (ε_1) for Case A and Case B. When conduction and convection heat transfer are considered, but radiative heat transfer on all inner surfaces facing airspaces is ignored ($\varepsilon_1 = \varepsilon_2 = 0.0$, Case B), Figure 10 indicates that the R_{eff} of the steel-framed wall with mass insulation is 0.660. This value is 56.9% greater than that of a wall without mass insulation (R_{eff} = 0.421, Figure 9). Additionally, for a wall with mass insulation, neglecting radiative heat transfer on the inner surface of Board-A while accounting for it on other inner surfaces (i.e., $\varepsilon_1 = 0.0$ and $\varepsilon_2 = 0.9$, Case A) results in a R_{eff} of 0.629, which is 80.7% higher than the value for a wall without mass insulation (R_{eff} = 0.347, Figure 9). For Case A in the hybrid system, using RI with ε_1 = 0.05 on the inner surface of Board-A facing the air cavity yields a R_{eff} of 0.606, representing an 88.0% increase over the wall without mass insulation (R_{eff} = 0.322, Case A in Figure 9). Similarly, for Case B in the hybrid system, applying RI with $\varepsilon_1 = \varepsilon_2 = 0.05$ to all inner surfaces facing airspaces in the steel-framed system achieves a R_{eff} of 0.643, which is 62.2% higher than that for a wall without mass insulation (R_{eff} = 0.396, Case B in Figure 9).

For a steel-framed wall incorporating mass insulation but lacking RI (i.e., $\varepsilon_1 = \varepsilon_2 = 0.9$), the calculated R_{eff} is 0.512. This value represents a significant improvement of 234.5% compared to a wall without mass insulation, where the R_{eff} is only 0.153. In contrast, for a wall without mass insulation but equipped with RI having ε_1 values of 0.03 and 0.05, respectively, and with ε_2 fixed at 0.9 (Case A in Figure 9), the values of R_{eff} are 0.331 and 0.322. These values are 35.4% and 37.1% lower than the R_{eff} for the wall with a

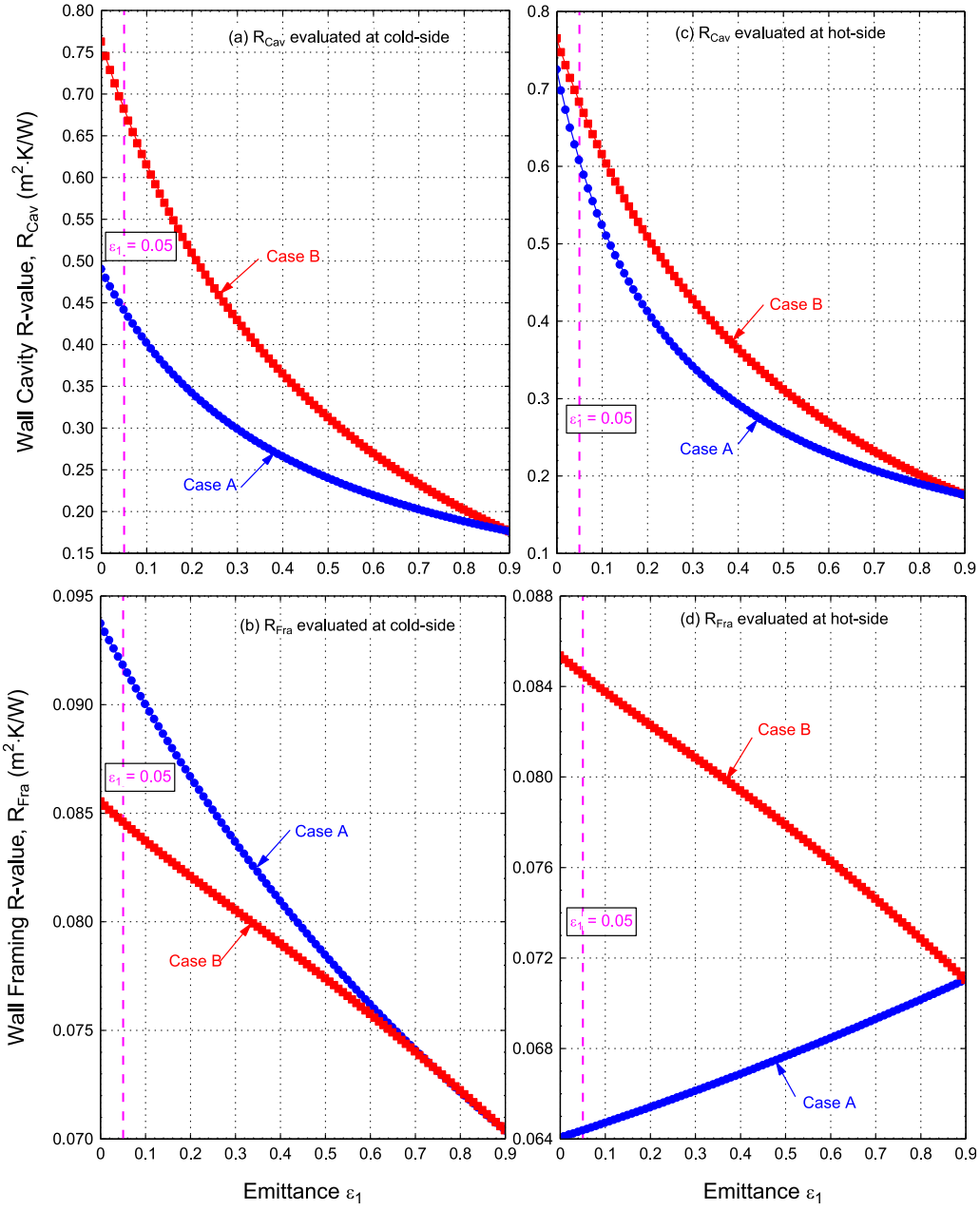

FIGURE 11
For the RIS, the dependences of R_{Cav} and R_{Fra} evaluated based on the cold and hot sides of the steel-framed wall on the emittance ε_1 for Cases A and B when: **(a)** wall cavity R-value evaluated at cold-side, **(b)** wall framing R-value evaluated at cold-side, **(c)** wall cavity R-value evaluated at hot-side, and **(d)** wall framing R-value evaluated at hot-side.

50.8-mm-thick mass insulation layer but without RI ($\varepsilon_1 = \varepsilon_2 = 0.9$). Alternatively, for walls without mass insulation but utilizing RI with $\varepsilon_1 = \varepsilon_2$ values of 0.03 and 0.05 (Case B in Figure 9), the R_{eff} values are 0.407 and 0.396, respectively. These results indicate reductions of only 20.6% and 22.7% relative to the R_{eff} of the wall with a 50.8-mm-thick mass insulation layer but without RI (R_{eff} = 0.512, Figure 10). These results highlight the thermal performance benefits of incorporating mass insulation in steel-framed walls with and without RI. Such insights can assist building designers in evaluating trade-offs between insulation types to optimize energy efficiency in building assemblies.

Reductions in thermal resistance of steel-framed systems due to thermal bridges

In steel-framed wall assemblies for both an RIS and a hybrid system, the presence of thermal bridges created by the steel components, including the C-shaped steel, top track, and bottom track (as illustrated in Figure 1), reduces the overall effective thermal resistance of the system. Within these steel framing elements, heat transfer occurs through all three modes: conduction, natural convection, and radiation, creating a complex three-dimensional thermal behavior. For a specified steel-framed system, the numerical

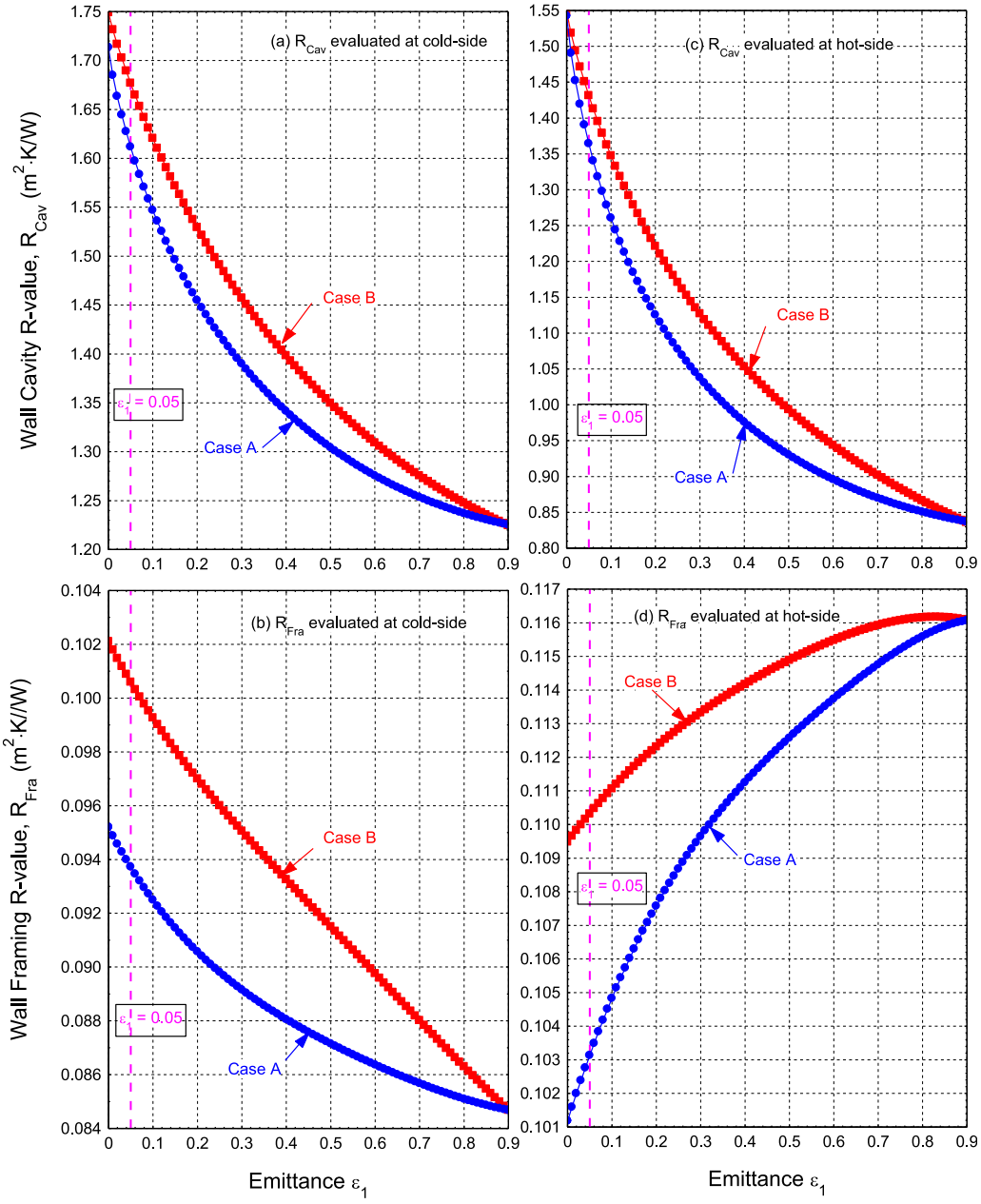

FIGURE 12
For the hybrid system, dependences R_{Cav} and R_{Fra} based on the cold and hot sides of the steel-framed wall on ε_1 for Cases A and B [δ_{ins} = 50.8 mm and k_{ins} = 0.04 W/(m·K)] when: **(a)** wall cavity R-value evaluated at cold-side, **(b)** wall framing R-value evaluated at cold-side, **(c)** wall cavity R-value evaluated at hot-side, and **(d)** wall framing R-value evaluated at hot-side.

results were analyzed for both an RIS and a hybrid system to evaluate the following thermal properties: (a) the effective thermal resistance (R_{eff}), calculated using either Equation 1 or Equation 12, as illustrated by the results in Figures 9, 10; (b) the framing thermal resistance (R_{Fra}) of the studs, top track, and bottom track (see Figure 4), determined using Equation 4; and (c) the wall cavity thermal resistance (R_{Cav}), assessed with and without the inclusion of reflective or mass insulation, calculated using Equation 8.

As previously discussed, the R_{eff} values derived based on the hot side of the assembly are the same as those obtained based on the cold side. However, the calculated values for R_{Fra} and R_{Cav} may vary depending on whether the hot-side or cold-side evaluation is used. For the R_{eff} results pertaining to the RIS shown in Figure 9, the corresponding values for R_{Cav} and R_{Fra} based on using the cold side are presented in Figures 11A,B, respectively, while the values for R_{Cav} and R_{Fra} based on using the hot side are displayed in Figures 11C,D, respectively. Similarly, for the hybrid system, whose R_{eff} results are illustrated in Figure 10, the evaluations of R_{Cav} and R_{Fra} based on using the cold side are provided in Figures 12A,B, respectively, while the corresponding evaluations based on using the hot side are shown in Figures 12C,D, respectively. These comprehensive analyses enable a detailed understanding of the

performance of steel-framed systems under varying configurations and conditions.

In RIS, for Case B in which $\varepsilon_1 = \varepsilon_2$, the calculated values of R_{Cav} and R_{Fra} based on the cold side (Figures 11A,B) are approximately the same as those calculated at the hot side (Figures 11C,D) for the whole range of emittance ε_1 of 0.0–0.9. At an emittance ε_1 of 0.05 as an example, the R_{Cav} calculated by Equation 8 and the R_{Fra} calculated by Equation 4, respectively, based on the hot side, are 0.683 and 0.085; whereas the R_{eff} calculated using either Equation 1 or Equation 12 is 0.396 (Figure 9). If no thermal bridges occur in such a building assembly, the resulting R_{eff} must equal R_{Cav}. The reduction in R_{eff} because of the framing thermal bridges due to studs and top and bottom racks (see Figure 4, where ξ = 10.2% in this study) is called R_{Red}, which is defined in this article as:

$$R_{Red} = R_{Cav} - R_{eff} \quad (13)$$

As the R_{eff} in Equation 13 evaluated based on the hot side is the same as that evaluated based on the cold side, when:

a. R_{cav} is evaluated based on the hot side; the corresponding R_{Red} is also based on the hot side, and
b. R_{Cav} is evaluated based on the cold side; the corresponding R_{Red} is also based on the cold side.

Thus, the values of R_{Red} based on the cold side could be different than those based on the hot side. For Case B ($\varepsilon_1 = \varepsilon_2$) in the RIS, to quantify the effect of thermal bridges at the emittance ε_1 of 0.05 (as example), the R_{eff} has reduced from R_{Cav} based on the hot side of 0.683 (Figure 11C) to 0.396 (Figure 9), which represents a reduction in R_{eff} by R_{Red} of 0.287 (72%) due to the effect of thermal bridges. Additionally, at the emittance ε_1 of 0.9 (i.e., wall assembly without RI), the R_{eff} has reduced from R_{Cav} based on the hot side of 0.176 (Figure 11C) to 0.153 (Figure 9), which represents a reduction in R_{eff} by R_{Red} of 0.023 (15%) due to the effect of thermal bridges. As such, the effect of thermal bridges resulted in a greater reduction in the R_{eff} at low emittance (e.g., 72% reduction at ε_1 = 0.05) than that at high emittance (e.g., 15% reduction at ε_1 = 0.9).

In the RIS, unlike Case B ($\varepsilon_1 = \varepsilon_2$), in which the evaluated R_{Cav} and R_{Fra} based on the hot side and the cold side are approximately the same, the evaluated R_{Cav} based on the hot side for Case A (ε_2 = 0.9) (Figure 11C) is higher than that evaluated based on the cold side (Figure 11A). Conversely, the evaluated R_{Fra} based on the hot side (Figure 11D) for Case A is lower than that evaluated based on the cold side (Figure 11B). As such, the amount of heat leaving the wall cavity at the cold side is more than that entering the wall cavity at the hot side; but the amount of heat leaving the steel frame (studs and top and bottom racks) at the cold side is less than that entering the steel frame at the hot side. However, the total amount of heat rate leaving the full steel-framed assembly at the cold side is the same as that entering the full assembly at the hot side due to energy conservation. For example, for Case A at emittances ε_1 of 0.0 and 0.05, respectively, R_{Cav} values based on the hot side (0.724 and 0.599, Figure 11C) are 49% and 37% higher than those evaluated based on the cold side (0.490 and 0.442, Figure 11A). Alternatively, at emittances ε_1 of 0.0 and 0.05, respectively, R_{Fra} values based on the hot side (0.0641 and 0.0643, Figure 11D) are 32% and 30% lower than those evaluated based on the cold side (0.0937 and 0.0918, Figure 11B). At these emittance values (i.e., 0.0 and 0.05), the corresponding values for R_{eff} are 0.347 and 0.322, respectively (Figure 9).

In the RIS when the evaluated R_{Cav} is based on the cold side for Case A at emittances ε_1 of 0.0 and 0.05, respectively, the R_{eff} values have reduced from R_{Cav} of 0.490 and 0.442 (Figure 11A) to 0.347 and 0.322 (Figure 9), which represents a reduction in R_{eff} by R_{Red} of 0.143 and 0.120 (41% and 37%) due to the effect of thermal bridges. Correspondingly, with the evaluated R_{Cav} based on the hot side at same emittance values ε_1 (i.e., 0.0 and 0.05, respectively) the R_{eff} values have reduced from R_{Cav} of 0.724 and 0.608 (Figure 11C) to 0.347 and 0.322 (Figure 9), which represents a reduction in R_{eff} by R_{Red} of 0.377 and 0.285 (109% and 89%) due to the effect of thermal bridges. With the whole range of emittance ε_1, however, increasing ε_1 from 0.0 to 0.9 resulted in: (a) decreasing the values of R_{Cav} based on the cold side from 0.490 to 0.176 (a reduction of 178%, Figure 11A), (b) decreasing the values of R_{Cav} based on the hot side from 0.724 to 0.176 (a reduction of 311%, Figure 11C), (c) decreasing the values of R_{Fra} based on the cold side from 0.0937 to 0.0704 (a reduction of 33%, Figure 11B), and (d) increasing the values of R_{Fra} based on the hot -side from 0.0641 to 0.0711 (an increase of 10%, Figure 11D).

For a hybrid system incorporating a mass thermal insulation 50.8 mm thick with a k_{ins} of 0.04 W/(m·K), Figure 12 shows the dependence of R_{Cav} and R_{Fra} based on the cold side and the hot side of a steel-framed wall on the emittance ε_1 for Case A (ε_2 = 0.9) and Case B ($\varepsilon_1 = \varepsilon_2$). For a given emittance ε_1 in both Case A and Case B, Figures 12A,C show that the R_{Cav} values based on the cold side are higher than those based on the hot side. Conversely, for a given emittance ε_1 in both Case A and Case B, Figures 12B,D show that the R_{Fra} values based on the cold side are lower than those based on the hot side. As such, the amount of heat leaving the wall cavity (refer to the dashed red box in Figure 2) at the cold side is less than that entering the wall cavity at the hot side. However, the amount of heat leaving the steel framing, shown in Figure 4, at the cold side is more than that entering the steel framing at the hot side. Whereas for a full steel-framed wall assembly, the total amount of heat leaving at the cold side is the same as that entering at the hot side due to energy conservation.

Note that at emittance ε_1 of 0.9, the thermal resistances of R_{eff}, R_{Cav}, and R_{Fra} for Case A are the same as those for Case B. To show the effect of the emittance ε_1 on these resistances for the hybrid system, increasing the emittance ε_1 from 0.0 to 0.9 for Cases A and B resulted in

a. Decreasing R_{Cav} based on the cold side from 1.714 to 1.226 (a reduction of 40%) for Case A and from 1.749 to 1.226 (a reduction of 43%) for Case B (Figure 12A).
b. Decreasing R_{Cav} based on the hot side from 1.543 to 0.837 (a reduction of 84%) for Case A and from 1.548 to 0.837 (a reduction of 85%) for Case B (Figure 12C).
c. Decreasing R_{Fra} based on the cold side from 0.0953 to 0.0847 (a reduction of 12%) for Case A and from 0.1021 to 0.0847 (a reduction of 21%) for Case B (Figure 12B).
d. Increasing R_{Fra} based on the hot side from 0.1013 to 0.1161 (an increase of 13%) for Case A and from 0.1095 to 0.1161 (an increase of 6%) for Case B (Figure 12D).

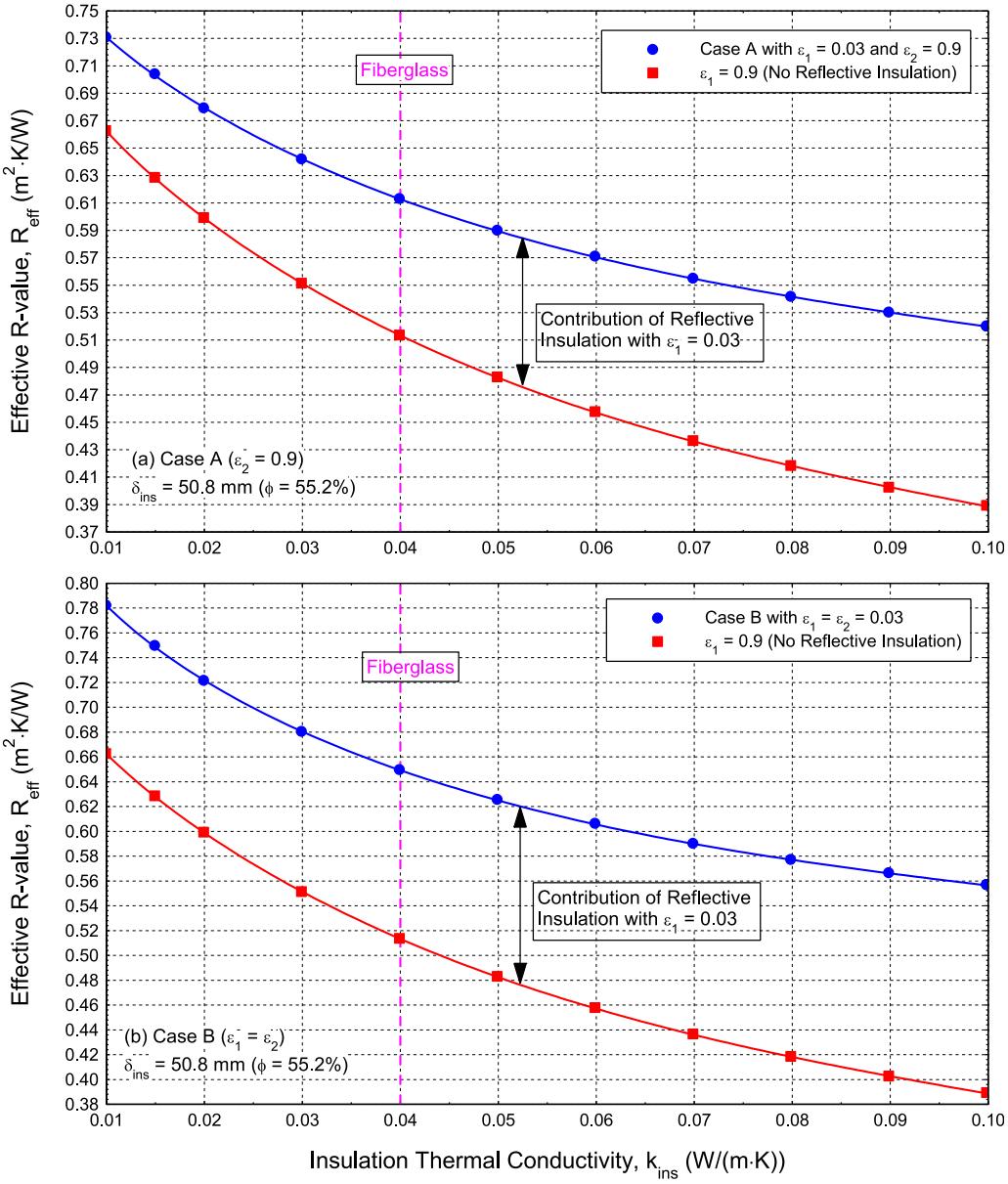

FIGURE 13
The effect of k_{ins} on R_{eff} for Cases A and B in the hybrid system with δ_{ins} = 50 mm.

e. Decreasing R_{eff} based on both the cold side and the hot side from 0.627 to 0.512 (a reduction of 22%) for Case A and from 0.660 to 0.512 (a reduction of 29%) for Case B (Figure 10).

To quantify the impact of thermal bridges of a steel frame on the effective thermal resistance of the hybrid system, when R_{Cav} is evaluated based on the cold side for Cases A and B at emittance values ε_1 of 0.0 and 0.05, respectively (as examples), the R_{eff} values have reduced: (a) from R_{Cav} of 1.714 and 1.611 (Figure 12A) to 0.627 and 0.763 (Figure 10), which represent reductions in R_{eff} by R_{Red} of 1.090 and 1.006 (174% and 166%) for Case A, and (b) from R_{Cav} of 1.749 and 1.677 (Figure 12A) to 0.660 and 0.643 (Figure 10), which represent reductions in R_{eff} by R_{Red} of 1.088 and 1.034 (165% and 161%) for Case B. Similarly, with the evaluated R_{Cav} based on the hot side at same emittance values ε_1 (i.e., 0.0 and 0.05, respectively) the R_{eff} values have reduced: (a) from R_{Cav} of 1.543 and 1.365 (Figure 12C) to 0.627 and 0.606 (Figure 10), which represent reductions in R_{eff} by R_{Red} of 0.916 and 0.759 (146% and 125%) for Case A, and (b) from R_{Cav} of 1.548 and 1.432 (Figure 12C) to 0.627 and 0.606 (Figure 10), which represent reductions in R_{eff} by R_{Red} of 0.921 and 0.826 (147% and 136%) for Case B.

In closing, the results demonstrated that thermal bridging induced by steel framing, specifically due to studs, top track, and bottom track, led to a substantial reduction in the R_{eff} of steel-framed wall assemblies. This effect was observed in both the RIS and the hybrid system in which the wall cavity was partially filled with fiberglass insulation at a filling ratio of ϕ = 55.2%.

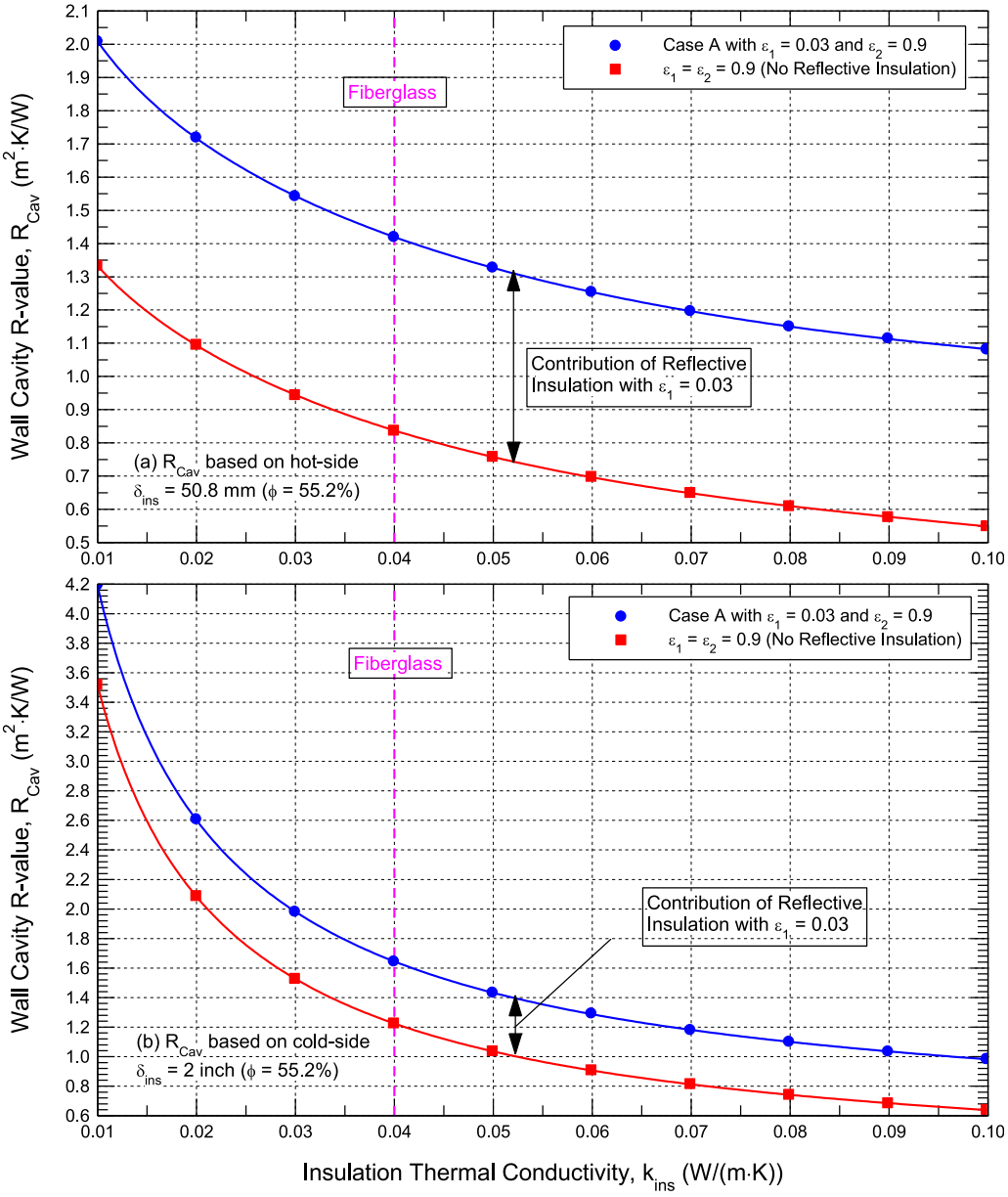

FIGURE 14
For Case A in the hybrid system with δ_{ins} = 50.8 mm, the effect of k_{ins} on R_{Cav} evaluated based on both the hot and cold sides.

Effect of mass insulation types on thermal resistance of hybrid systems

This section discusses the impact of mass insulation types on the performance of a steel-framed wall system. The results provided in this study cover the range of k_{ins} available in the market, which is 0.01–0.10. Note that for a given insulation type, the k_{ins} at the dry condition could increase at a wet condition (i.e., high moisture content) and/or due to deterioration of the insulation material. An example of filling a wall cavity with 50.8-mm-thick thermal insulation installed on the inner surface of Board-B (see Figure 1) is considered in this study to explore the impact of mass insulation type on thermal resistances of hybrid systems for both Case A (ε_2 = 0.9) and Case B ($\varepsilon_1 = \varepsilon_2$). The scenario of mass insulation with 50.8 mm thickness corresponds to filling the wall cavity with mass insulation by ϕ = 55.2%. It is important to point out that each figure conveys distinct insights: Figures 13–15 highlight the role of insulation type on the effective and wall cavity thermal resistances; Figures 16–18 examine the influence of insulation filling ratio on the effective thermal resistances; and Figures 19–24 assess the combined effects of insulation properties with and without reflective insulation on the wall cavity thermal resistances evaluated based on both the cold side and the hot side. Collectively, these figures illustrate different but complementary aspects of thermal behavior, thereby justifying the inclusion of a wide range of cases.

With RI at an emittance ε_1 of 0.03 and without RI (i.e., ε_1 = 0.9), Figures 13A,B show the effects of mass insulation types on R_{eff} for

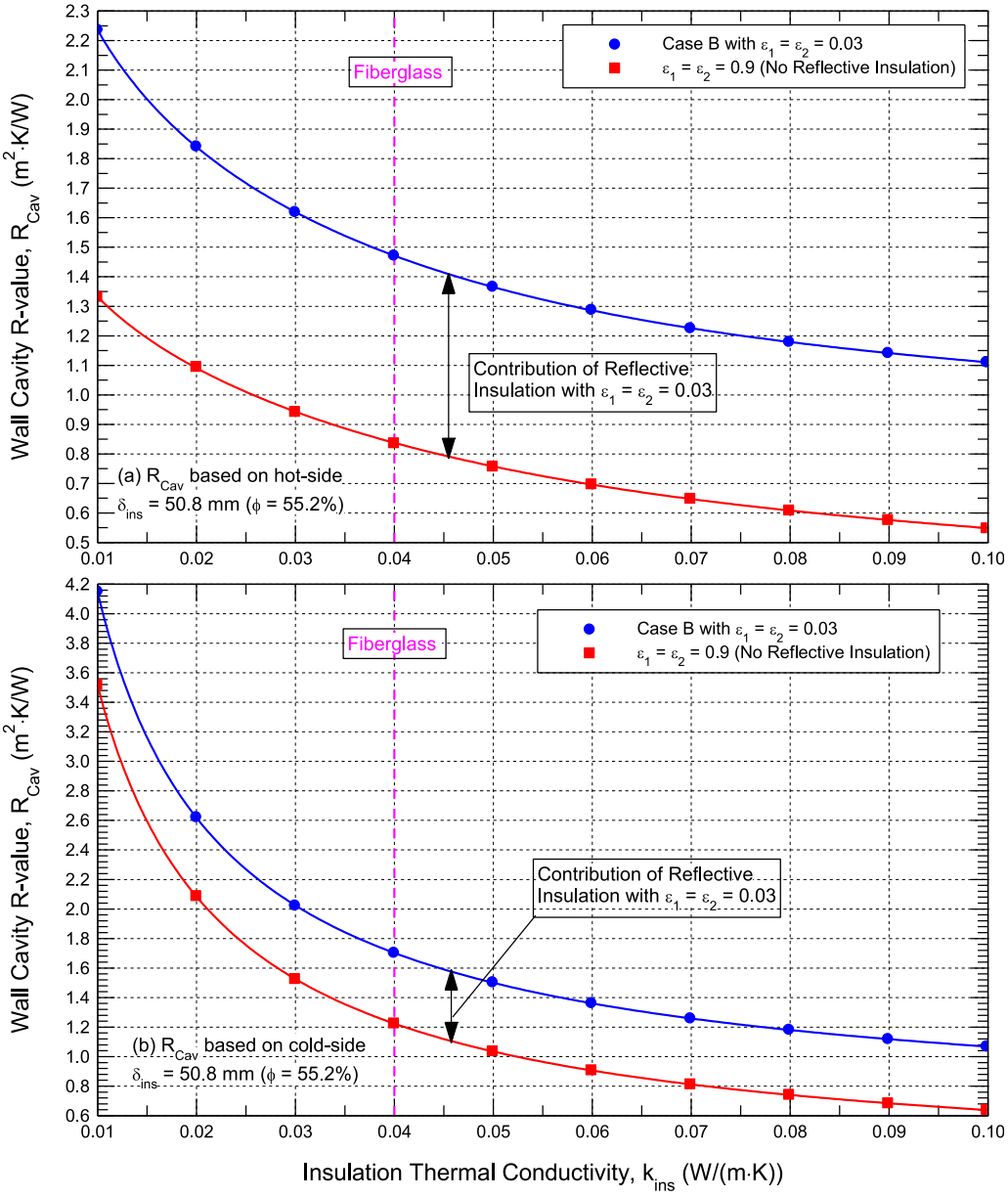

FIGURE 15
For Case B in the hybrid system with δ_{ins} = 50.8 mm, the effect of k_{ins} on R_{Cav} evaluated based on both the hot and the cold sides.

Case A and Case B, respectively. The corresponding results showing the effects of insulation types on the thermal resistances of the wall cavity (R_{Cav}) when they are calculated based on the hot and cold sides are provided in Figures 14, 15 for Case A and Case B, respectively.

As shown in Figures 13–15, the results of R_{eff} and R_{Cav} at the emittance ε_1 of 0.9 are the same for both Cases A and B, which represent the scenario of steel-framed wall assemblies without RI. For a given insulation type (i.e., a given k_{ins} value) at emittance ε_1 = 0.03 (as an example), the amounts of increase in the R_{eff} and R_{Cav} values beyond those at emittance ε_1 of 0.9 represent the contributions of installing RI in the steel-framed assemblies. For a steel-framed system without RI (ε_1 = 0.9), Figures 13A,B show that increasing k_{ins} from 0.01 to 0.10 resulted in decreasing R_{eff} from 0.662 to 0.389, which represents a reduction in R_{eff} of 70%. Similarly, at the emittance ε_1 of 0.9, Figures 14, 15 show that increasing k_{ins} from 0.01 to 0.10 resulted in decreasing the evaluated R_{Cav} based on the hot side and the cold side, respectively, from 1.333 to 0.549 (a reduction in R_{Cav} of 143%), and from 3.519 to 0.638 (a reduction in R_{Cav} of 452%).

Figure 13A for Case A in the hybrid system shows that decreasing the emittance ε_1 from 0.9 to 0.03 at a low k_{ins} value of 0.01 resulted in increasing R_{eff} from 0.662 to 0.731, which represents an increase in R_{eff} of 10%. However, decreasing the emittance ε_1 from 0.9 to 0.03 at a high k_{ins} value of 0.10 resulted in increasing R_{eff} from 0.389 to 0.520, which represents a larger increase in R_{eff} value of 33% compared to 10% at a low k_{ins} value of 0.01. In addition, decreasing the emittance ε_1 from 0.9 to 0.03 at a

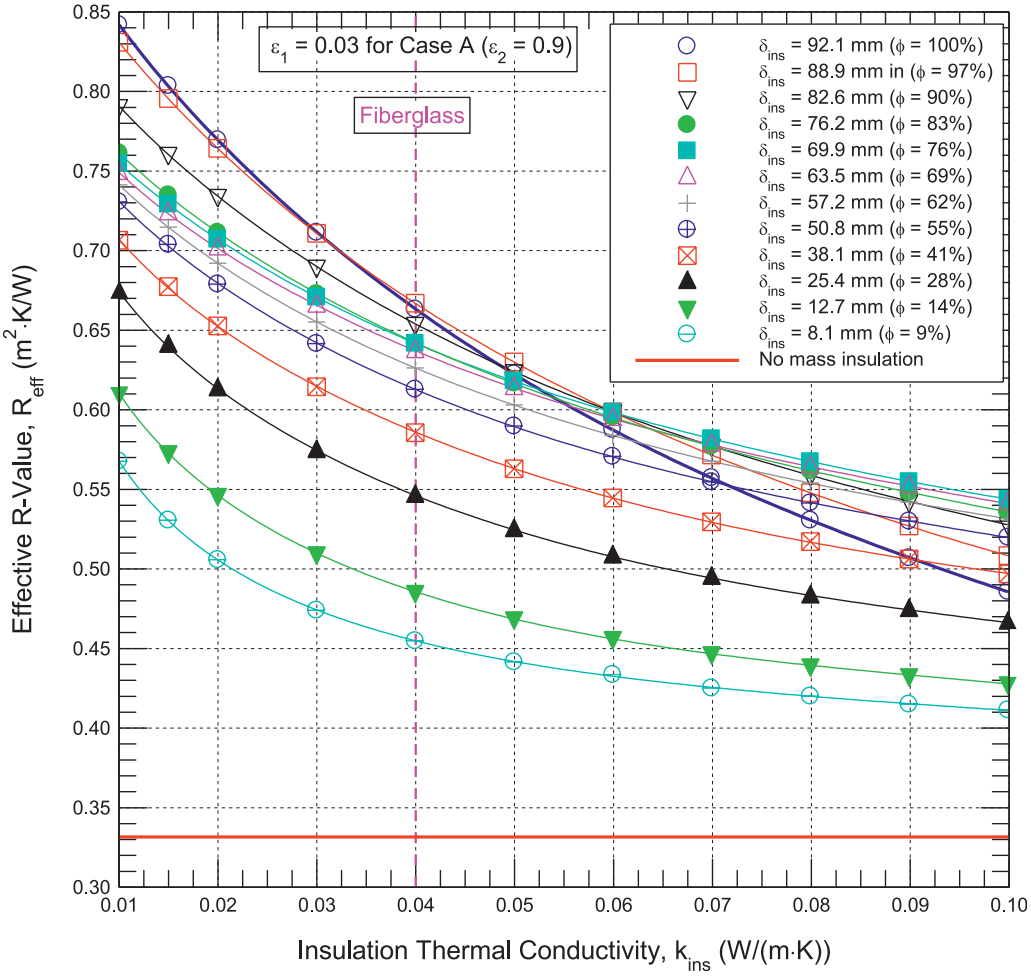

FIGURE 16
The effect of the mass insulation filling ratio on R_{eff} for Case A at emittance ε_1 = 0.03.

low k_{ins} value of 0.01 resulted in increasing the evaluated R_{Cav} from 1.333 to 2.009 based on the hot side (an increase in R_{Cav} of 51%, Figure 14A), and from 3.519 to 4.191 based on the cold side (an increase in R_{Cav} of 19%, Figure 14B). Whereas decreasing the emittance ε_1 from 0.9 to 0.03 at a high k_{ins} value of 0.10 resulted in increasing the evaluated R_{Cav} from 0.549 to 1.081 based on the hot side, which represents an increase in R_{Cav} of 97% compared to 51% at k_{ins} = 0.01 (Figure 14A), and from 0.638 to 0.983 based on the cold side, which represents a 54% increase in R_{Cav} compared to 19% at k_{ins} = 0.01 (Figure 14B).

For Case B in the hybrid system, Figure 13B shows that decreasing the emittance ε_1 from 0.9 to 0.03 at a low k_{ins} value of 0.01 increases the value of R_{eff} from 0.662 to 0.782 (i.e., an 18% increase in R_{eff} compared to 10% for Case A shown in Figure 13A). At a high k_{ins} value of 0.10 for Case B, however, decreasing the emittance ε_1 from 0.9 to 0.03 increases R_{eff} from 0.389 to 0.557 (i.e., a 43% increase in R_{eff} compared to 33% for Case A shown in Figure 13A). Furthermore, Figures 15A,B for Case B show that decreasing the emittance ε_1 from 0.9 to 0.03 at a low k_{ins} value of 0.01 increases the evaluated R_{Cav} from 1.333 to 2.237 based on the hot side (a 68% increase in R_{Cav} compared to 51% for Case A shown in Figure 14A), and from 3.519 to 4.151 based on the cold side (an 18% increase in R_{Cav} compared to 19% for Case A shown in Figure 14B). However, for Case B at the high k_{ins} value of 0.10, Figures 15A,B show that decreasing the emittance ε_1 from 0.9 to 0.03 increases the evaluated R_{Cav} from 0.549 to 1.111 based on the hot side (a 102% increase in R_{Cav} compared to 97% for Case A shown in Figure 14A), and from 0.638 to 1.069 based on the cold side (a 68% increase in R_{Cav} compared to 54% for Case A shown in Figure 14B).

In summary, using RI with low-e (e.g., see Figures 13–15 for ε_1 = 0.03) for Case A of hybrid systems with mass thermal insulation of high thermal conductivity resulted in a greater increase in both R_{eff} and R_{Cav} compared to the mass thermal insulation of low thermal conductivity. The corresponding increase in these thermal resistances (R_{eff} and R_{Cav}) for Case B ($\varepsilon_1 = \varepsilon_1$) is greater than that for Case A (ε_1 = 0.9).

Effect of mass insulation filling ratio on effective thermal resistance of steel-framed systems

Numerical simulations were conducted for steel-framed wall systems when the wall cavity between the steel studs was filled with different quantities of thermal mass insulation of various types.

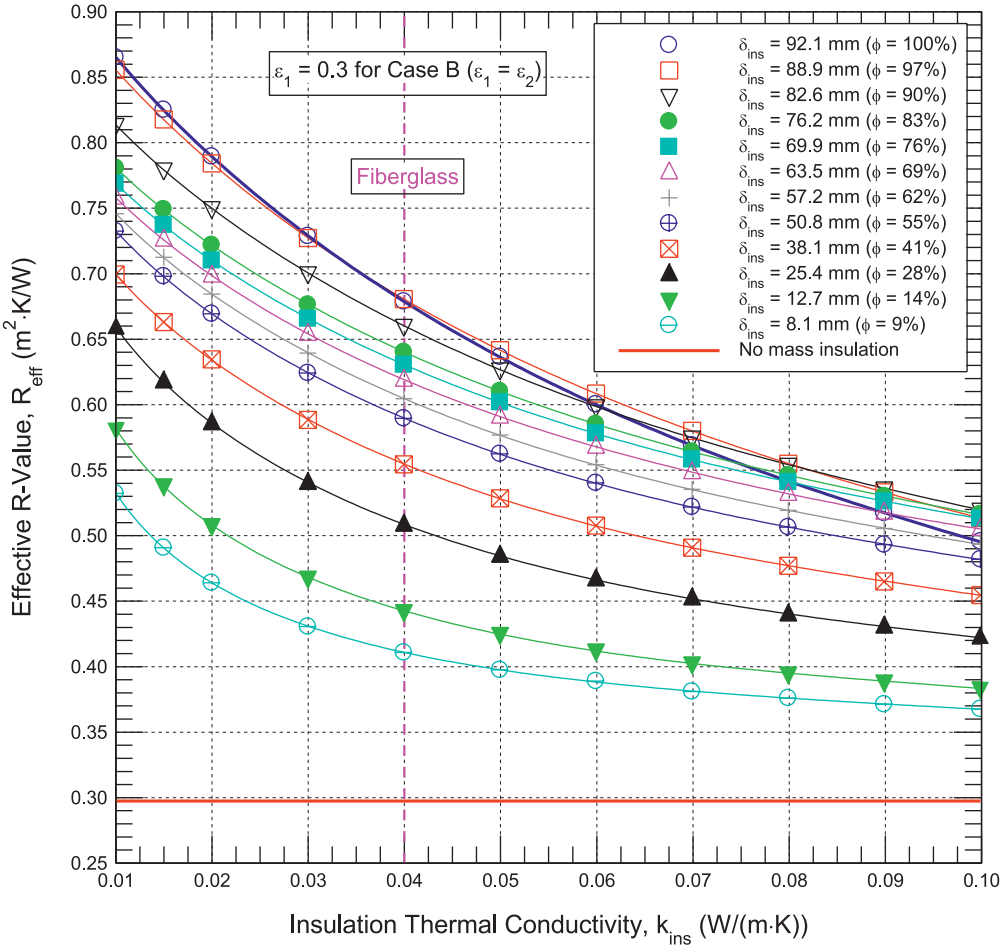

FIGURE 17
The effect of the mass insulation filling ratio on R_{eff} for Case B at emittance ε_1 = 0.03.

These simulations were conducted for both Case A (ε_2 = 0.9) and Case B (ε_1 = ε_2) over a range of insulation filling ratios, ϕ of 0%–100%. For Case A at an emittance ε_1 of 0.03, Figure 16 shows the effect of insulation filling ratio on the R_{eff} of the steel-framed walls. In addition, Figure 17 shows the effect of ϕ on R_{eff} for Case B (ε_1 = ε_2 = 0.03). As a reference, the effect of ϕ on the R_{eff} of the steel-framed walls without RI for both Cases A and B (i.e., ε_1 = ε_2 = 0.9) is also shown in Figure 18. For future use in updating the "Design Guide titled Thermal Design and Code Compliance for Cold-Formed Steel Walls (American Iron and Steel Institute, 2015) to include various types of RIs, the corresponding R_{eff} results for other emittance ε_1 values are provided in Supplementary Appendix–A: (a) Figure A - 1 (ε_1 = 0.05), Figure A - 2 (ε_1 = 0.1) and Figure A - 3 (ε_1 = 0.3) for Case A, and (b) Figure A - 4 (ε_1 = ε_2 = 0.05), Figure A - 5 (ε_1 = ε_2 = 0.1) and Figure A - 6 (ε_1 = ε_2 = 0.3).

As a result of increasing k_{ins} from 0.01 to 0.10, the value of ϕ = 100% represents the scenario of a wall cavity completely filled with mass insulation for which the R_{eff} value at ε_1 = 0.03 has decreased from 0.842 to 0.486 for Case A (a reduction in R_{eff} by 73%, Figure 16) and from 0.884 to 0.504 for Case B (a reduction in R_{eff} by 76%, Figure 17). Additionally, for the same filling ratio (i.e., ϕ = 100%) but without RI (ε_1 = ε_2 = 0.9), Figure 18 shows that R_{eff} has decreased from 0.817 to 0.475 (a reduction in R_{eff} by 72%) as a result of increasing k_{ins} from 0.01 to 0.10. However, the value of ϕ = 0% represents the scenario of no mass insulation used in the wall cavity for which the values R_{eff} at ε_1 = 0.03 are 0.331 for Case A (Figure 16) and 0.407 for Case B (Figure 17); whereas without RI (ε_1 = ε_2 = 0.9), the corresponding R_{eff} is 0.153 (Figure 18).

For both Cases A and B, Figures 16, 17 indicate that when k_{ins} values are relatively low, the effective thermal resistance (R_{eff}) at ϕ = 100% consistently exceeds that of cases where ϕ < 100%. Conversely, at higher k_{ins} values, R_{eff} at ϕ = 100% may become lower than in cases with ϕ < 100%. To examine this behavior more closely, a new parameter, k^*_{ins}, is introduced. This parameter represents the thermal conductivity of mass insulation at which the effective thermal resistance (R_{eff}) and the wall cavity thermal resistance (R_{Cav}) evaluated at the hot and cold sides of steel-framed wall systems are identical for configurations with ϕ = 100% and those with a lower amount of mass insulation (ϕ < 100%). The k^*_{ins} value can thus serve as an indicator for identifying the type of mass insulation in these systems.

For Case A at ε_1 = 0.03, Figure 16 shows that at k^*_{ins} values of 0.048, 0.062, 0.072, and 0.091, the values of R_{eff} for ϕ = 100% are 0.629, 0.579, 0.553, and 0.505, respectively; whereas these R_{eff} values are achieved with a smaller amount of mass insulation at ϕ of 90%, 62%, 55%, and 41%, respectively. For k_{ins} > k^*_{ins} at these ϕ values, the

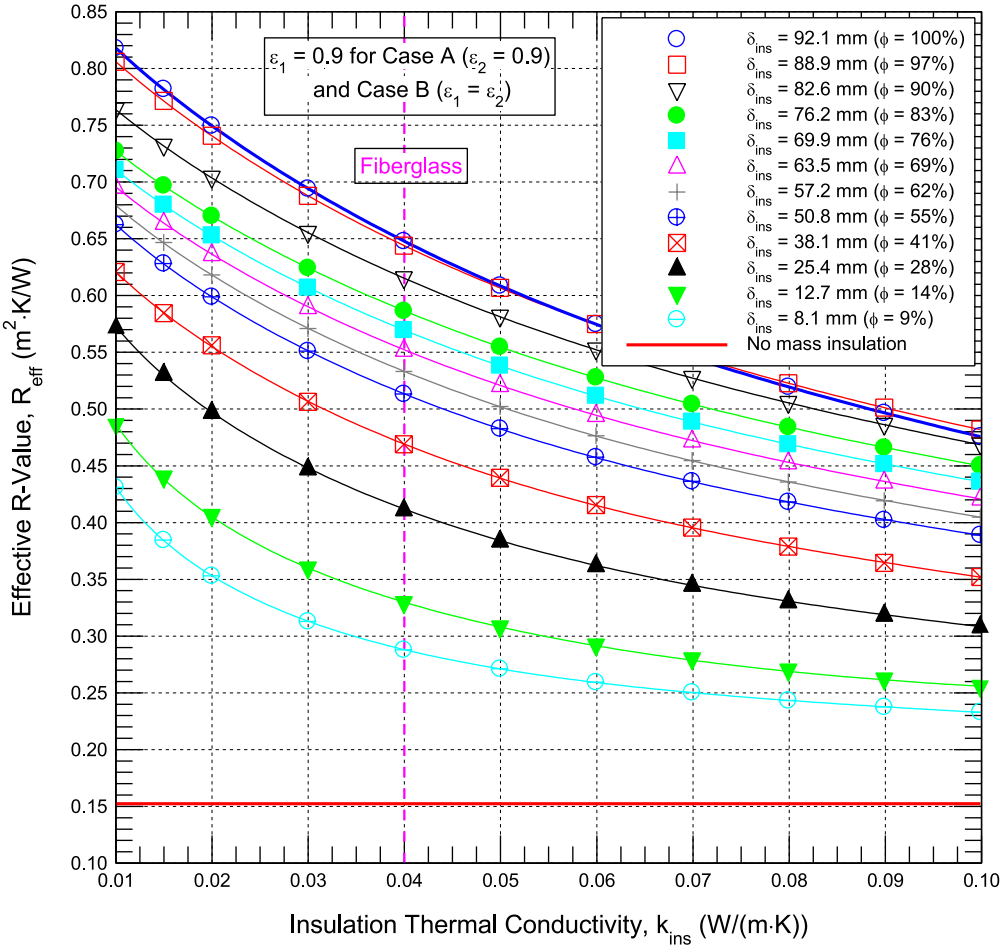

FIGURE 18
The effect of the mass insulation filling ratio on R_{eff} for Cases A and B without RI ($\varepsilon_1 = \varepsilon_1 = 0.9$).

R_{eff} values are larger than those with ϕ of 100%. For example, at k_{ins} of 0.10 and ϕ of 62%, the R_{eff} value (0.532) is 9% larger than that for ϕ of 100% (0.486). At the k^*_{ins} values of 0.048, 0.056, 0.063, 0.076, and 0.095, Figure 17 for Case B at $\varepsilon_1 = \varepsilon_2 = 0.03$ shows that the R_{eff} values for ϕ = 100% are 0.660, 0.623, 0.601, 0.560, and 0.514, respectively, which are the same as those in a steel-framed wall with a smaller amount of mass insulation at ϕ of 90%, 62%, 55%, 41%, and 28%, respectively. Similar to Case A, when $k_{ins} > k^*_{ins}$ at these ϕ values for Case B, the R_{eff} values are larger than those with ϕ of 100%. For example, at k_{ins} of 0.10 and ϕ of 62%, the R_{eff} value (0.565) is 12% larger than that for ϕ of 100% (0.504). In other words, a larger R_{eff} value can be achieved in a steel-framed wall with less mass insulation than in a steel-framed wall in which the cavity is completely filled with mass thermal insulation (i.e., ϕ = 100%).

In summary, when k_{ins} is low, a fully insulated cavity (ϕ = 100%) resulted in a higher R_{eff} than partial fillings (ϕ < 100%). However, at higher k_{ins} values, partially filled walls exhibited greater R_{eff} than completely filled ones. The threshold k^*_{ins} was identified as the critical thermal conductivity value where R_{eff} for ϕ = 100% is equal to that of walls with less insulation. This suggests that strategically adjusting insulation levels can improve the thermal performance of a steel-framed system while also lowering insulation material costs.

Effect of the mass insulation filling ratio on the wall cavity thermal resistance of steel-framed systems

As indicated earlier, the ASTM C1224 standard for reflective insulation in building assemblies outlines an approach to separate the impact of framing thermal bridges from the overall effective thermal resistance of the assembly to allow for the determination of the RI thermal resistance (ASTM, 2021). Following the same ASTM C1224 approach, this study excludes the effects of thermal bridging due to studs and top and bottom tracks in steel-framed systems. These exclusions are applied to cases with and without RI, and with and without mass insulation, to evaluate the wall cavity thermal resistance (R_{Cav}). As previously discussed, the evaluated R_{eff} based on the cold side of the steel-framed wall assembly is equivalent to that based on the hot side, where the R_{eff} results are provided in Figures 16–18 and Figure A - 1 through Figure A - 6. However, the R_{Cav} may vary depending on whether it is calculated using the cold side or the hot side. For both Cases A and B, this section discusses the influence of different types of mass insulation with various filling ratios on the R_{Cav} of steel-framed wall systems, considering scenarios with and without RI.

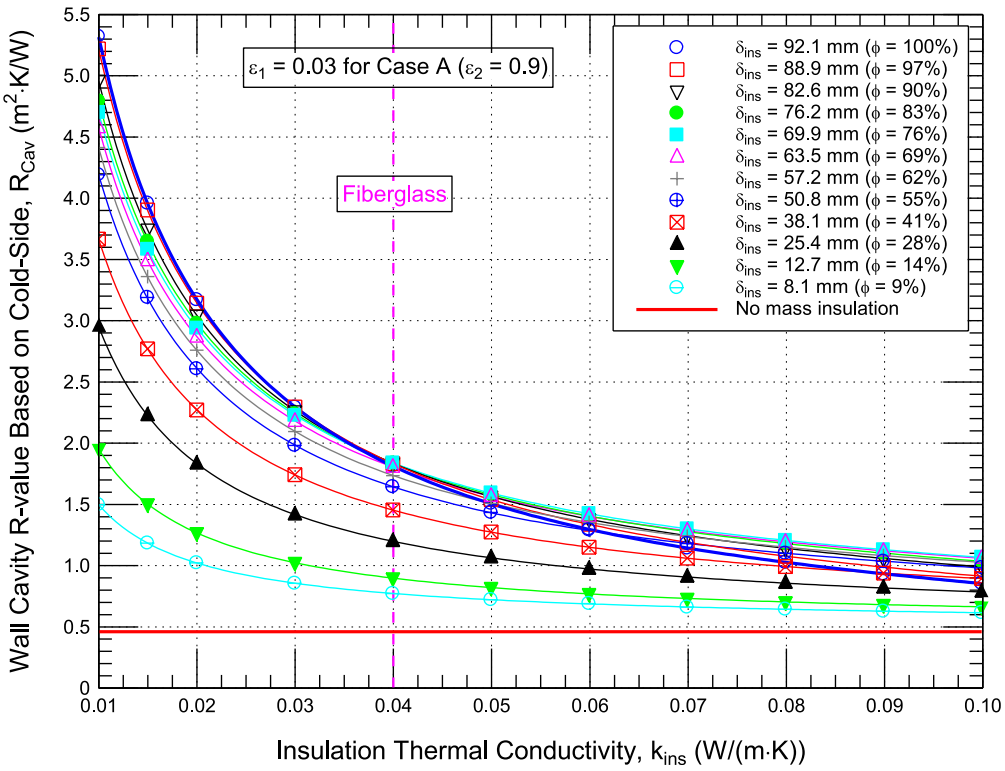

FIGURE 19
The effect of the mass insulation filling ratio on R_{Cav} based on the cold side of steel-framed walls for Case A at emittance ε_1 = 0.03.

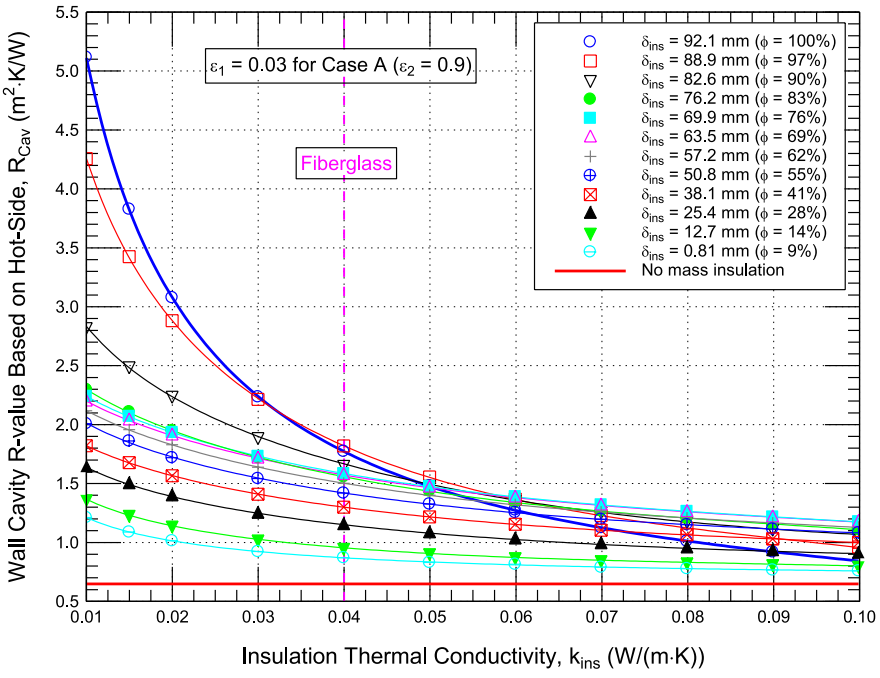

FIGURE 20
The effect of the mass insulation filling ratio on R_{Cav} based on the hot side of steel-framed walls for Case A at emittance ε_1 = 0.03.

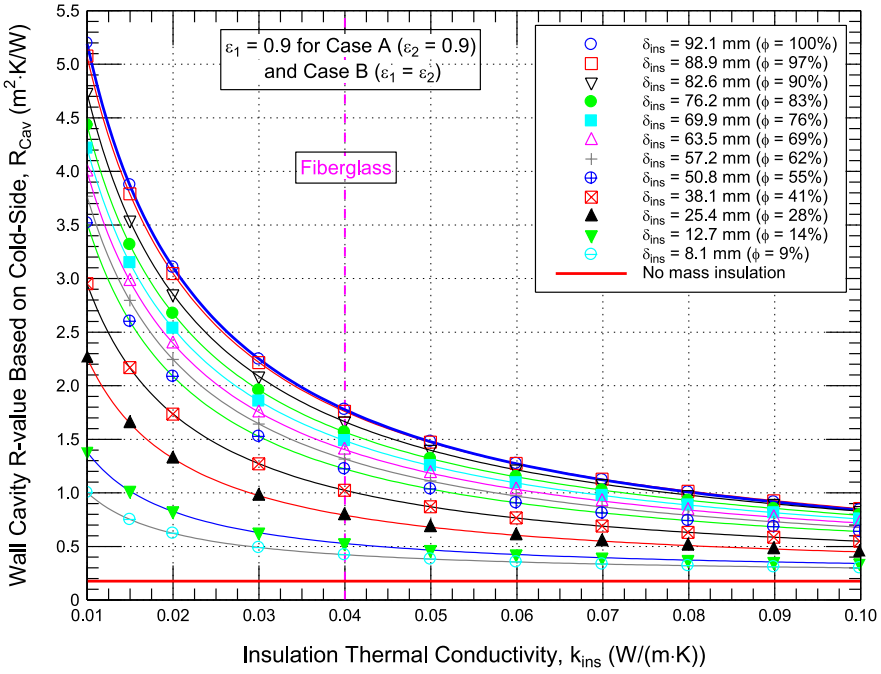

FIGURE 21
The effect of the mass insulation filling ratio on R_{Cav} based on the cold side of steel-framed walls for Cases A and B without RI (ε_1 = ε_2 = 0.9).

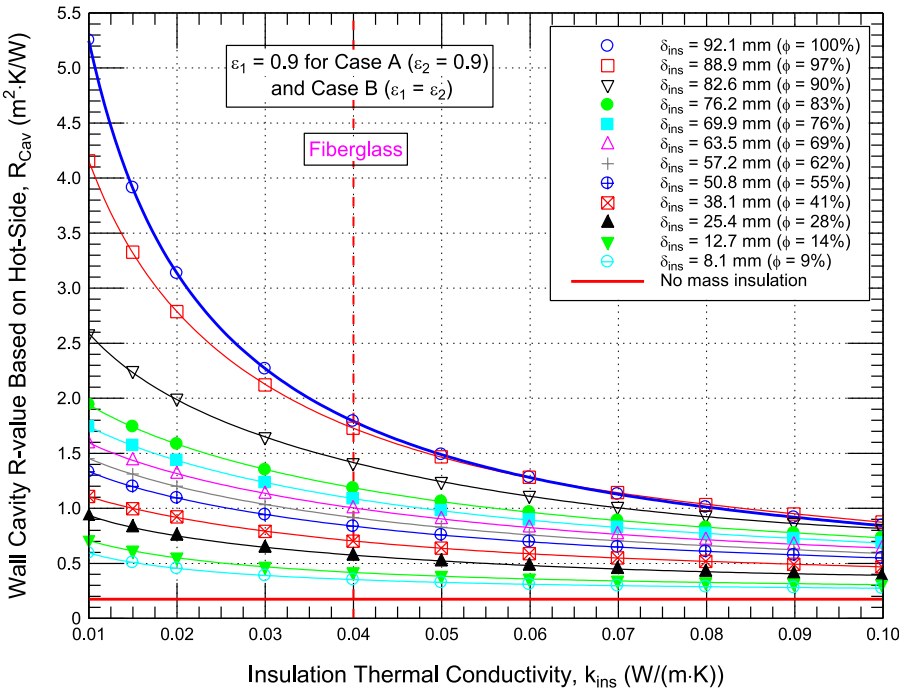

FIGURE 22
The effect of the mass insulation filling ratio on R_{Cav} based on the hot side of steel-framed walls for·Cases A and B without RI (ε_1 = ε_2 = 0.9).

For Case A (ε_2 = 0.9) at emittance ε_1 of 0.03, Figures 19, 20 show the effect of k_{ins} (i.e., type of mass insulation) and insulation filling ratio on the evaluated R_{Cav} based on the cold side and the hot side, respectively. For future use in upgrading the Design Guide of steel-framed walls (American Iron and Steel Institute, 2015), the corresponding results at other ε_1 values are provided in Supplementary Appendix–A for the evaluated R_{Cav} based on the cold side (see Figure A - 7 at ε_1 = 0.05, Figure A - 8 at ε_1 = 0.1, and Figure A - 9 at ε_1 = 0.3), and for the

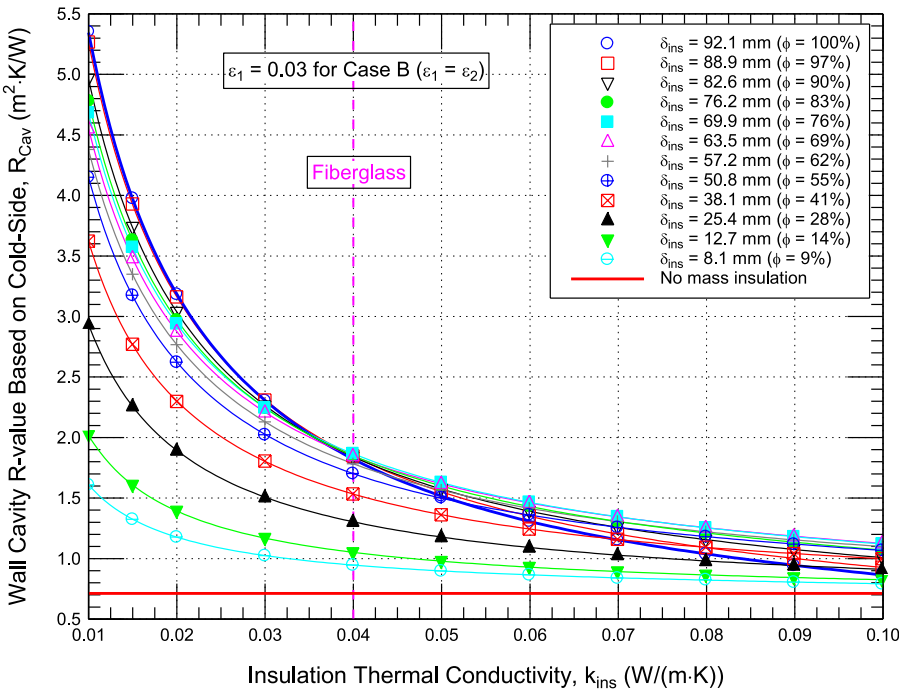

FIGURE 23
The effect of the mass insulation filling ratio on R_{Cav} based on the cold side of steel-framed walls for Case B at emittance ε_1 = ε_2 = 0.03.

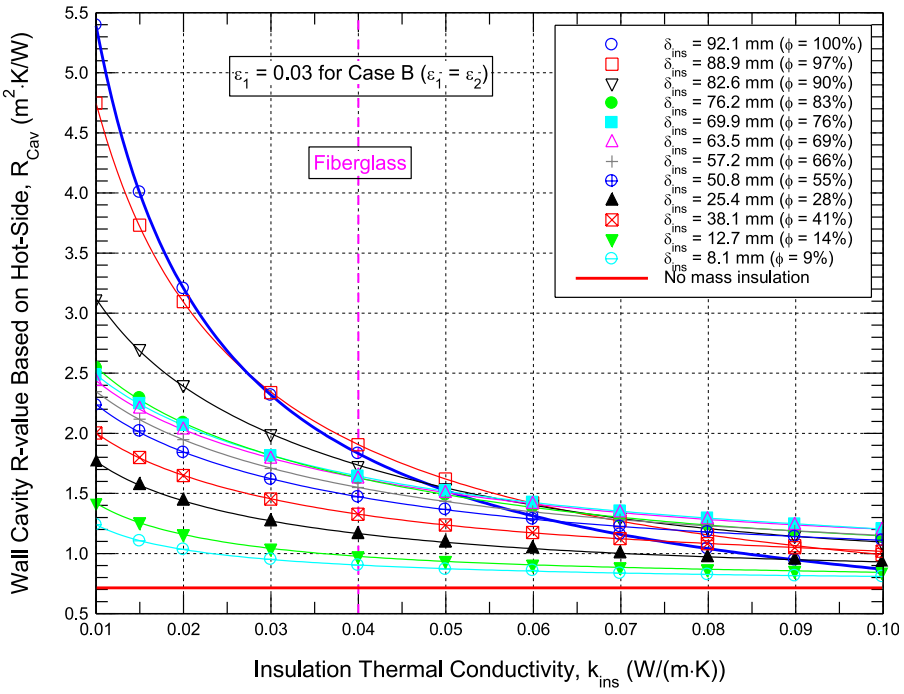

FIGURE 24
The effect of the mass insulation filling ratio on R_{Cav} based on the hot side of steel-framed walls for Case B at emittance ε_1 = ε_2 = 0.03.

evaluated R_{Cav} based on the hot side (see Figure A - 10 at ε_1 = 0.05, Figure A - 11 at ε_1 = 0.1, and Figure A - 12 at ε_1 = 0.3). In addition, to show the effect of not installing RI in the steel-framed wall system (i.e., ε_1 = ε_1 = 0.9), Figures 21, 22, respectively, show the impact of the type and filling ratio of mass insulation on the evaluated R_{Cav} based on the cold side and the hot side.

Without mass insulation, Figures 19, 20, respectively, show that the evaluated R_{Cav} based on the cold and hot sides at $\varepsilon_1 = 0.03$ are 0.460 and 0.650, which are 0.460 and 0.657 times those without RI (see Figures 21, 22). With mass insulation of various filling ratios, and with and without RI, Figures 19–22 show that the R_{Cav} increases with decreasing k_{ins}. Furthermore, due to decreasing k_{ins}, the rate of increasing R_{Cav} (i.e., dR_{Cav}/dk_{ins}) is greater within the range of low k_{ins} values than it is within the range of large k_{ins} values. For example, within the range of low k_{ins} values of a steel-framed wall system with RI at $\varepsilon_1 = 0.03$, and filling the wall cavity with mass insulation of 25.4 mm thickness (i.e., $\phi = 28\%$), the evaluated R_{Cav} values based on the cold side and the hot side, respectively, have increased 2.77 times or by 177% (from 1.064 to 2.952, Figure 19), and 1.52 times or by 52% (from 1.078 to 1.636, Figure 20) due to decreasing k_{ins} from 0.05 to 0.01 (i.e., $\Delta k_{ins} \approx 0.04$. However, within the same range of $\Delta k_{ins} \approx 0.04$ but with large k_{ins} values at these conditions (i.e., $\varepsilon_1 = 0.03$ and $\phi = 28\%$), the R_{Cav} values have increased by only 35% (from 0.785 to 1.064 based on the cold side, Figure 19), and only 19% (from 0.905 to 1.078 based on the hot side, Figure 20) as a result of decreasing k_{ins} from 0.10 to 0.05.

At $\phi = 28\%$ with a low k_{ins} value of 0.01 but without RI ($\varepsilon_1 = 0.9$), Figures 21, 22 show that the evaluated R_{Cav} values at the cold side and the hot side, respectively, are 2.259 and 0.933. Incorporating RI in the same steel-framed wall at $\varepsilon_1 = 0.03$, however, resulted in: (a) increasing R_{Cav} based on the cold side from 2.259 to 2.952 (an increase in R_{Cav} of 31%), and (b) increasing R_{Cav} based on the hot side from 0.933 to 1.636 (an increase in R_{Cav} of 75%). Correspondingly, at $\phi = 28\%$ with a large k_{ins} value of 0.10 but without RI, the evaluated R_{Cav} values based on the cold side and the hot side, respectively, are 0.449 and 0.389. With RI at $\varepsilon_1 = 0.03$, these values have increased to 0.785 based on the cold side (an increase in R_{Cav} of 75%) and to 0.905 based on the hot side (an increase in R_{Cav} of 133%). Consequently, using RI in a steel-framed wall system with mass thermal insulation of large thermal conductivity resulted in a larger increase in the wall cavity thermal resistance compared to mass insulation of low thermal conductivity.

In closing, for Case A with RI at $\varepsilon_1 = 0.03$ and mass insulation with $\phi = 28\%$ (as an example), a 75% increase in R_{Cav} based on the cold side has been achieved at large k_{ins} of 0.10 *versus* 31% at a low k_{ins} of 0.01. Under these conditions, a 133% increase in R_{Cav} based on the hot side has been achieved at a large k_{ins} *versus* 75% at a low k_{ins}.

Regarding Case B ($\varepsilon_1 = \varepsilon_2$) at emittance ε_1 of 0.03, Figures 23, 24 show the effect of k_{ins} and insulation filling ratio ϕ on R_{Cav} when it is evaluated based on the cold side and the hot side, respectively. At other ε_1 values, the corresponding results are provided in the Supplementary Appendix–A for R_{Cav} evaluated based on the cold side in Figure A - 13 at $\varepsilon_1 = 0.05$, Figure A - 14 at $\varepsilon_1 = 0.1$, and Figure A - 15 at $\varepsilon_1 = 0.3$. Additionally, the results for the evaluated R_{Cav} based on the hot side are provided in Figure A - 16 at $\varepsilon_1 = 0.05$, Figure A - 17 at $\varepsilon_1 = 0.1$, and Figure A - 18 at $\varepsilon_1 = 0.3$.

At $\varepsilon_1 = \varepsilon_2 = 0.03$, Figures 23, 24 show that the R_{Cav} values for a steel frame without mass insulation when they are evaluated based on the cold side and the hot side, respectively, are 0.711 and 0.713, which are 55% and 10% higher than those for Case A at $\varepsilon_1 = 0.03$ (0.460 and 0.650, Figures 21, 22). Similar to Case A with mass insulation, the rate of increasing R_{Cav} for Case B due to decreasing k_{ins} is greater within the range of low k_{ins} values than within the range of large k_{ins} values. For instance, within the range of low k_{ins} values at $\phi = 90\%$ for Case B at $\varepsilon_1 = \varepsilon_2 = 0.03$, decreasing k_{ins} from 0.05 to 0.01 ($\Delta k_{ins} \approx 0.04$) resulted in the evaluated R_{Cav} based on the cold side and the hot side, respectively, increasing by 3.387, as shown in Figure 23 (*versus* 3.332 for Case A at $\varepsilon_1 = 0.03$; Figure 19), and by 1.573, as shown in Figure 24 (*versus* 1.338 for Case A at $\varepsilon_1 = 0.03$, Figure 20). On the other hand, within the same range of $\Delta k_{ins} \approx 0.04$ but at large k_{ins} values, Figure 23 shows that decreasing k_{ins} from 0.10 to 0.05 resulted in increasing the evaluated R_{Cav} based on the cold side by only 0.567 for Case B at $\varepsilon_1 = \varepsilon_2 = 0.03$ (*versus* 0.571 for Case A at $\varepsilon_1 = 0.03$, Figure 19) and increasing the evaluated R_{Cav} based on the hot side by only 0.453 for Case B at $\varepsilon_1 = \varepsilon_2 = 0.03$ (Figure 24) compared 0.394 for Case A at $\varepsilon_1 = 0.03$ (Figure 20).

As shown in Figures 19, 20 for Case A at $\varepsilon_1 = 0.03$ and Figures 23, 24 for Case B at $\varepsilon_1 = \varepsilon_2 = 0.03$, the same wall cavity thermal resistance value of a steel-framed wall system in which the wall cavity is completely filled with mass thermal insulation ($\phi = 100\%$) can be achieved with a smaller amount of mass insulation as a result of using RI. As stated earlier, in this condition, the mass insulation thermal conductivity corresponds to a critical threshold value (k^*_{ins}). At $\phi = 100\%$ for Case A, Figure 19 shows that the evaluated R_{Cav} based on the cold side of 1.779, 1.508, 1.266, and 0.946, respectively, can also be achieved with a smaller amount of mass insulation at: (a) $\phi = 69\%$ with $k^*_{ins} = 0.041$, (b) $\phi = 62\%$ with $k^*_{ins} = 0.050$, (c) $\phi = 55\%$ with $k^*_{ins} = 0.062$, and (d) $\phi = 41\%$ with $k^*_{ins} = 0.088$. Similarly, at $\phi = 100\%$ for Case A, the evaluated R_{Cav} based on the hot side of 1.458, 1.349, 1.242, 6.21, and 0.926, respectively, can also be achieved with less insulation at: (a) $\phi = 69\%$ with $k^*_{ins} = 0.051$, (b) $\phi = 62\%$ with $k^*_{ins} = 0.056$, (c) $\phi = 55\%$ with $k^*_{ins} = 0.062$, (d) $\phi = 41\%$ with $k^*_{ins} = 0.073$, and (e) $\phi = 28\%$ with $k^*_{ins} = 0.089$ (see Figure 20).

Similar to Case A, Figure 23 shows that the R_{Cav} values for Case B at $\phi = 100\%$ based on the cold side of 1.918, 1.691, 1.463, 1.155, and 0.944, respectively, can be achieved with less insulation at: (a) $\phi = 69\%$ with $k^*_{ins} = 0.037$, (b) $\phi = 62\%$ with $k^*_{ins} = 0.044$, (c) $\phi = 55\%$ with $k^*_{ins} = 0.052$, (d) $\phi = 41\%$ with $k^*_{ins} = 0.070$, and (e) $\phi = 28\%$ with $k^*_{ins} = 0.090$ (Figure 23). As shown in Figure 24, the corresponding R_{Cav} values for Case B at $\phi = 100\%$ based on the hot side are 1.493, 1.370, 1.268, 1.106, and 0.949, respectively, which can also be achieved at: (a) $\phi = 69\%$ with $k^*_{ins} = 0.051$, (b) $\phi = 62\%$ with $k^*_{ins} = 0.057$, (c) $\phi = 55\%$ with $k^*_{ins} = 0.063$, (d) $\phi = 41\%$ with $k^*_{ins} = 0.074$, and (e) $\phi = 28\%$ with $k^*_{ins} = 0.090$.

To close, for the scenarios analyzed above, increasing k_{ins} beyond its corresponding critical threshold k^*_{ins} leads to the wall cavity thermal resistance for cases with less insulation ($\phi < 100\%$) exceeding that of the fully insulated case ($\phi = 100\%$). This finding highlights the complex interplay between the properties of reflective and mass insulation and the performance of steel-framed systems. The results presented in this study, encompassing both the effective thermal resistance and the wall cavity thermal resistance for steel-framed wall systems with and without RI, and with varying insulation filling ratios, offer valuable insights for building engineers and professionals. These findings can provide a robust foundation for designing cost-effective steel-framed wall systems that optimize thermal performance. By leveraging these results, practitioners can achieve a balance between the properties of reflective and mass insulation, performance, and regulatory compliance in steel-framed construction.

Future work

This study has shown that thermal bridging caused by steel framing results in a significant reduction in the effective thermal resistance of steel-framed wall assemblies. This phenomenon was evident in both the reflective insulation system (RIS) and the hybrid system, where the wall cavity was partially or completely filled with mass insulation. The complex, three-dimensional heat transfer within steel-framed assemblies is governed by a combination of conduction, convection, and radiation. To increase the effective thermal resistance of these assemblies, it is essential to reduce heat transfer through the framing components, thereby mitigating the adverse effects of thermal bridging. A potential strategy to address thermal bridging involves eliminating convective and radiative heat transfer within the steel framing components. This can be achieved by filling the structural elements, such as studs, top track, and bottom track, with mass thermal insulation materials. Thus, a follow-up study is currently underway to investigate the impact of filling steel framing components with various types of mass thermal insulation on the effective thermal resistance of wall assemblies in both RISs and hybrid systems, incorporating different types and quantities of insulation within the wall cavity. Potential candidates for this purpose include spray-applied open-cell foam, spray-applied closed-cell foam, fiberglass, expanded polystyrene (EPS), extruded polystyrene (XPS), and similar insulation products. The goal is to identify configurations that maximize thermal performance while maintaining practical constructability. The results of this comprehensive investigation will provide further insights into mitigating thermal bridging and increasing energy efficiency in steel-framed wall assemblies. These findings will be disseminated in forthcoming publications.

Summary and conclusion

This study examined the performance of steel-framed assemblies incorporating reflective insulation (RI) under standard labeling conditions (an average temperature of 23.9 °C and a temperature difference of 16.6 °C). The RI configurations, collectively referred to as the reflective insulation system (RIS), were evaluated in two scenarios: Case A, where RI was installed on a single board on the hot side with its reflective surface facing the airspace, and Case B, where RI was applied to all internal surfaces facing airspaces within the wall assembly. Both Case A and Case B provide insights into the thermal behavior of steel-framed walls under varying configurations. The findings provide valuable guidance for building designers in selecting between these configurations to develop cost-effective steel-framed wall systems. Additionally, the study investigated hybrid systems, which integrate RI with different quantities of mass insulation in the wall cavity, covering a wide range of thermal conductivity values. A validated three-dimensional numerical model was employed to analyze the thermal performance of both RIS and hybrid systems. Because RI products typically exhibit emittance values between 0.03 and 0.2 but may increase due to either dust accumulation and/or moisture condensation, the study accounted for a range of emittance (ε_1) values from 0 to 0.9.

In an RIS, the results demonstrated that RI significantly increases the effective thermal resistance (R_{eff}) of steel-framed wall assemblies. For an emittance of 0.05, R_{eff} increased by approximately 2.1 times for Case A and 2.6 times for Case B compared to wall systems without RI, with Case B showing a 23.0% greater improvement than Case A. In hybrid systems with 50.8-mm-thick fiberglass insulation that corresponds to an insulation filling ratio of 55% (as an example), R_{eff} was 88.0% higher for Case A and 62.2% higher for Case B than the RIS alone. Conversely, compared to steel-framed walls with fiberglass insulation without RI, R_{eff} values for RIS were 37.1% lower for Case A and 22.7% lower for Case B. To comply with ASTM C1224, the study also introduced a method to separate the impact of thermal bridging due to steel framing components, such as studs, top tracks, and bottom tracks, allowing for evaluating the thermal resistance of wall cavities in RISs and hybrid systems.

This study demonstrates that incorporating reflective insulation with low emittance in steel-framed walls affects thermal resistance based on the thermal conductivity of mass insulation. For low-conductivity insulation, completely filled wall cavities provide higher thermal resistance than partially filled ones. However, as conductivity increases, partially filled cavities outperform fully insulated configurations, with a critical threshold, referred to as $k^*_{ins}$where thermal resistance values become equivalent. Beyond this point, walls with reduced insulation can achieve greater thermal resistance than those with fully insulated cavities. These findings highlight the complex interaction between reflective and mass insulation in steel-framed construction, offering valuable guidance for optimizing thermal efficiency while reducing material costs. This research provides engineers with a framework for designing cost-effective, high-performance wall systems that effectively balance insulation properties, energy efficiency, and compliance with regulatory requirements.

Overall, the findings highlight the impact of thermal bridging on the performance of steel-framed systems and the thermal efficiency benefits of combining various forms of reflective insulation with different types and quantities of mass insulation available on the market. As current design guidelines, such as "Thermal Design and Code Compliance for Cold-Formed Steel Walls," do not account for RI, this study provides essential data to support updates to these guidelines, facilitating the integration of RISs and hybrid systems into thermal design practices for steel-framed building assemblies.

Last but not least, the novelty of this research lies in its comprehensive evaluation of reflective insulation systems and hybrid insulation systems in steel-framed wall assemblies using a validated three-dimensional model. Unlike previous studies, this work introduces an ASTM C1224–based methodology for isolating thermal bridge effects, identifies a previously unreported critical thermal conductivity threshold that determines whether partial or full cavity insulation is more effective, and quantifies the impact of RISs and hybrid systems on thermal resistance across a wide range of emittance values. These findings not only fill a major knowledge gap but also provide a scientific foundation for updating current design guidelines and building codes to incorporate reflective insulation technologies, both with and without conventional mass insulation.

Data availability statement

The original contributions presented in the study are included in the article/Supplementary Material; further inquiries can be directed to the corresponding author.

Author contributions

HS: Conceptualization, Data curation, Formal Analysis, Funding acquisition, Investigation, Methodology, Project administration, Resources, Software, Supervision, Validation, Visualization, Writing – original draft, Writing – review and editing.

Funding

The author(s) declare that no financial support was received for the research and/or publication of this article.

Acknowledgments

This work did not receive any specific grant or funding from public, commercial, or non-profit organizations. AI was used solely for language and grammar checks in certain sentences, all of which were carefully reviewed by the author to ensure factual accuracy and originality. No generative AI tools were employed to produce scientific content, perform data analysis, or interpret results. The author assumes full responsibility for the integrity and accuracy of the manuscript.

Conflict of interest

The author declares that the research was conducted in the absence of any commercial or financial relationships that could be construed as a potential conflict of interest.

The author(s) declared that they were an editorial board member of Frontiers, at the time of submission. This had no impact on the peer review process and the final decision.

Generative AI statement

The author(s) declare that Generative AI was used in the creation of this manuscript. Solely for language and grammar checks in certain sentences, and these were carefully reviewed by the author to ensure factual accuracy and originality. No generative AI tools were employed to create scientific content, perform data analysis, or interpret results. AI is not listed as an author, and its use is disclosed in the Acknowledgments section of the manuscript.

Any alternative text (alt text) provided alongside figures in this article has been generated by Frontiers with the support of artificial intelligence and reasonable efforts have been made to ensure accuracy, including review by the authors wherever possible. If you identify any issues, please contact us.

Publisher's note

Supplementary material

The Supplementary Material for this article can be found online at: https://www.frontiersin.org/articles/10.3389/fmech.2025.1689473/full#supplementary-material

References

American Iron and Steel Institute (2015). *Thermal design and code compliance for cold-formed steel walls*. Washington, DC: Steel Framing Alliance. Available online at: https://www.cfsei.org/assets/docs/designguides/thermal_design_guide_2015_edition.pdf.

ASHRAE (2017). *Handbook of fundamentals*. Atlanta, GA: ASHRAE International.

ASTM (1953). *Astm C236: test method for thermal conductance and transmittance of built-up sections by means of a guarded hot box*. Philadelphia, PA, United States: American Society for Testing and Materials.

ASTM (2003). *ASTM C518. Standard test method for steady-state heat flux measurements and thermal transmission properties by means of the heat flow meter apparatus*. Philadelphia, PA: ASTM, 153–164.

ASTM (2020a). *ASTM C1371: standard test method for determination of emittance of materials near Room temperature using portable emissometers*. Book of Standards Volume: 04.06. Developed by Subcommittee: C16.30. West Conshohocken, PA: American, Society for Testing and Materials.

ASTM (2020b). *ASTM C1363. Standard test method for the thermal performance of building assemblies by means of a hot box apparatus annual book of ASTM standards vol. 04.04*. Philadelphia, PA: ASTM, 793–837.

ASTM (2021). *Astm C1224: standard specification for reflective insulation for building applications volume 04.06*. West Conshohocken, PA: ASTM-International, 706–710.

Barbour, E., Goodrow, J., Kosny, J., and Christian, J. E. (1994). Thermal performance of steel-framed walls. Final report. Report number: DOE/OR/21400-T484; ON: DE96000665; CRN: C/ORNL--93-0235. Oak ridge national lab. (ORNL), Oak ridge, TN; NAHB research center, Inc., upper Marlboro, MD; Holometrix, Inc., Bedford, MA. Available online at: https://www.osti.gov/biblio/111848 (Accessed February 15, 2025).

CMHC (2004). *Glass and metal curtain walls, best practice guide building technology, ISBN 0-660-19394-9, Cat. No. NH15-428/2004E*. Canada: Canada Mortgage and Housing Corporation CMHC.

Fricker, J. M., and Yarbrough, D. W. (2011). "Review of reflective insulation estimation methods," in Proceedings of building simulation. Sydney, Australia: 12th conference of international building performance simulation association, 14–16 November 2011, 1989–1996. Available online at: https://publications.ibpsa.org/conference/paper/?id=bs2011_1640.

Ge, H., and Baba, F. (2017). Effect of dynamic modeling of thermal bridges on the energy performance of residential buildings with high thermal mass for cold climates. *Sustain. Cities Soc.* 34, 250–263. doi:10.1016/j.scs.2017.06.016

Gorgolewski, M. (2007). Developing a simplified method of calculating U-values in light steel framing. *Build. Environ.* 42 (1), 230–236. doi:10.1016/j.buildenv.2006.07.001

Hens, H. (2007). *Building physics: fundamentals and engineering methods with examples and exercises*. Berlin: Ernst a Sohn.

Iea, A. X. I. I. (1987). *International energy agency, energy conservation in buildings and community systems programme, annex XII, windows and fenestration, step 2, thermal and solar properties of windows, expert guide*. Delft, Netherlands: TNO Institute of Applied Physics.

IECC (2018). *International energy conservation code*. Country Club Hills, IL: International Code Council.

Kosny, J., and Desjarlais, A. O. (1994). Influence of architectural details on the overall thermal performance of residential wall systems. *J. Therm. Insulation Build. Envelopes, VIII* 18, 53–69. doi:10.1177/109719639401800104

Kosny, J., and Yarbrough, D. W. (2022). "Thermal efficiency of insulation in building structures—the impact of thermal bridging," in *Book: thermal insulation and radiation control technologies for buildings* (Cham, Switzerland: Springer International Publishing), 443–486. doi:10.1007/978-3-030-98693-3_15

Kosny, J., Christian, J. E., and Desjarlais, A. O. (1997). Thermal breaking systems for metal stud wall—can metal stud walls perform as well as wood stud walls? *ASHRAE Trans.* 103, 518–536. Available online at: https://www.scopus.com/inward/record.uri?eid=2-s2.0-0030698997&partnerID=40&md5=723efb9fa89cc80f963007a66117e66c.

Kosny, J., Yarbrough, D. W., Petrie, T., Childs, P., Mohiuddin, S. A., and Blair, C. (2007). *Nanoscale insulation at work. Thermal performance of thermally bridged wood and steel structures insulated with local aerogel insulation, X conference, thermal performance of the exterior envelopes of buildings, December*. Florida: Clearwater, 6.

Kośny, J., Curcija, C., Fontanini, A. D., Liu, H., and Kossecka, E. (2016). *A new approach for analysis of complex building envelopes in whole building energy simulations, buildings xiii – thermal performance of the exterior envelope of whole buildings conference*. Peachtree Corners, GA, United States: American Society of Heating, Refrigerating and Air-Conditioning Engineers (ASHRAE).

NCC (2021). National construction code, understanding the NCC thermal bridging, commonwealth of Australia and the states and Territories of Australia 2021, Australian Building Codes Board. Available online at: abcb.gov.au (Accessed January 10, 2025).

Robinson, H. E., Powlitch, F. J., and Dill, R. S. (1954). *The thermal insulation value of airspaces, 32*. Housing and Home Finance Agency. Available online at: https://www.govinfo.gov/content/pkg/GOVPUB-C13-e03d654909004ee8996d00ae3758b12a/pdf/GOVPUB-C13-e03d654909004ee8996d00ae3758b12a.pdf.

Roppel, P., Hershfield, M., and Marif, W. (2011). *Thermal performance of buildings envelope details for mid and high-rise buildings. ASHRAE research project report RP-1365*. Atlanta, GA: American Society of Heating, Refrigerating and Air-Conditioning Engineers, Inc. Article 30329.

Saber, H. H. (2012). Investigation of thermal performance of reflective insulations for different applications. *Build. Environ.* 52, 32–44. doi:10.1016/j.buildenv.2011.12.010

Saber, H. H., and Yarbrough, D. W. (2021). Advanced modeling of enclosed-airspaces to determine thermal resistance for building applications. *Energies* 14 (22), 7772. doi:10.3390/en14227772

Saber, H. H., and Yarbrough, D. W. (2023a). Assessing the effect of air intrusion on reflective insulations performance with horizontal heat flow. *Buildings* 13 (10), 2461. doi:10.3390/buildings13102461

Saber, H. H., and Yarbrough, D. W. (2023b). Determining the thermal resistance of enclosed reflective airspace. *Buildings* 13, 662. doi:10.3390/buildings13030662

Saber, H. H., Maref, W., Swinton, M. C., and St-Onge, C. (2011). Thermal analysis of above-grade wall assembly with low emissivity materials and furred-airspace. *Build. Environ.* 46 (7), 1403–1414. doi:10.1016/j.buildenv.2011.01.009

Saber, H. H. (2022). Overview of thermal performance of air cavities and reflective insulations. Thermal insulation and radiation control technologies for buildings (Green Energy and Technology), Editios J. Kośny and D. W. Yarbrough, ASIN: B0B3HN6W4J, publisher: Springer, ISSN: 1865-3529, ISSN: 1865-3537 (electronic), Green Energy and Technology ISBN: 978-3-030-98692-6, ISBN: 978-3-030-98693-3, Chapter 3, Pages 55–82, Gewerbestrasse 11, 6330 Cham, Switzerland.

Saber, H. H., Alshehri, S. A., and Yarbrough, D. W. (2024). Innovative airspace reflective tool for different building applications, Part I: tool development. *J. Sci. Technol. Built Environ.* 30 (7), 785–799. doi:10.1080/23744731.2024.2357527

Trechsel, H. R., and Bomberg, M. T. (2009). *Moisture control in buildings: the key factor in mold prevention*. West Conshohocken, PA: ASTM International. doi:10.1520/MNL18-2ND-EB

Trethowen, H. A. (1988). Thermal insulation and contact resistance in metal-framed panels. *ASHRAE Trans.* 94, 1802–1817. Available online at: https://api.semanticscholar.org/CorpusID:114783274.